Single and Binary Equilibrium Studies for Ni2+ and Zn2+ Biosorption onto Lemna gibba from Aqueous Solutions

Authors:

Liliana Morales-Barrera, César Mateo Flores-Ortiz, Eliseo Cristiani-Urbina

Date Submitted: 2021-02-22

Keywords: single and binary metal biosorption isotherm, Lemna gibba, pH and metal concentration effect, divalent zinc, divalent nickel, competitive biosorption

Abstract:

The biosorption ability of Lemna gibba for removing Ni2+ and Zn2+ ions in aqueous batch systems, both individually and simultaneously, was examined. The influences of solution pH and initial single and binary metal concentrations on equilibrium Ni2+ and Zn2+ biosorption was explored. The optimal solution pH for Ni2+ and Zn2+ biosorption was 6.0, for both the single and binary metal systems. Ni2+ and Zn2+ biosorption capacities increased with increasing initial metal concentrations. The presence of Zn2+ ions more adversely affected the biosorption of Ni2+ ions in the binary metal systems than vice versa. The single and binary biosorption isotherms of Ni2+ and Zn2+ revealed that L. gibba's affinity for Zn2+ ions was higher than that for Ni2+ ions. The Redlich?Peterson and Freundlich isotherm models fit well to the experimental equilibrium data of Ni2+ ions, whereas Redlich?Peterson and Langmuir models better described the equilibrium data of Zn2+ ions in single metal systems. The modified Sips isotherm model best fit the competitive biosorption data of Ni2+-Zn2+ on L. gibba. FTIR analyses suggest the involvement of hemicellulose and cellulose in the biosorption of Ni2+ and Zn2+. The presence of Ni2+ and Zn2+ on the L.gibba surface was validated by SEM-EDX.

Record Type: Published Article

Submitted To: LAPSE (Living Archive for Process Systems Engineering)

Citation (overall record, always the latest version):	LAPSE:2021.0079
Citation (this specific file, latest version):	LAPSE:2021.0079-1
Citation (this specific file, this version):	LAPSE:2021.0079-1v1

DOI of Published Version: https://doi.org/10.3390/pr8091089

processes

MDPI

Article

Single and Binary Equilibrium Studies for Ni^{2+} and Zn^{2+} Biosorption onto *Lemna gibba* from Aqueous Solutions

Liliana Morales-Barrera [1], César Mateo Flores-Ortiz [2,3] and Eliseo Cristiani-Urbina [1,*]

1 Departamento de Ingeniería Bioquímica, Escuela Nacional de Ciencias Biológicas, Instituto Politécnico Nacional, Ciudad de México 07738, Mexico; lilianamor@prodigy.net.mx
2 Laboratorio Nacional en Salud, Facultad de Estudios Superiores-Iztacala, Universidad Nacional Autónoma de México, Tlalnepantla, Estado de México 54090, Mexico; cmflores65@gmail.com
3 Unidad de Biotecnología y Prototipos, Facultad de Estudios Superiores-Iztacala, Universidad Nacional Autónoma de México, Tlalnepantla, Estado de México 54090, Mexico
* Correspondence: ecristiani@ipn.mx; Tel.: +52-55-5729-6000 (ext. 57835)

Received: 11 August 2020; Accepted: 31 August 2020; Published: 2 September 2020

Abstract: The biosorption ability of *Lemna gibba* for removing Ni^{2+} and Zn^{2+} ions in aqueous batch systems, both individually and simultaneously, was examined. The influences of solution pH and initial single and binary metal concentrations on equilibrium Ni^{2+} and Zn^{2+} biosorption was explored. The optimal solution pH for Ni^{2+} and Zn^{2+} biosorption was 6.0, for both the single and binary metal systems. Ni^{2+} and Zn^{2+} biosorption capacities increased with increasing initial metal concentrations. The presence of Zn^{2+} ions more adversely affected the biosorption of Ni^{2+} ions in the binary metal systems than vice versa. The single and binary biosorption isotherms of Ni^{2+} and Zn^{2+} revealed that *L. gibba*'s affinity for Zn^{2+} ions was higher than that for Ni^{2+} ions. The Redlich–Peterson and Freundlich isotherm models fit well to the experimental equilibrium data of Ni^{2+} ions, whereas Redlich–Peterson and Langmuir models better described the equilibrium data of Zn^{2+} ions in single metal systems. The modified Sips isotherm model best fit the competitive biosorption data of Ni^{2+}-Zn^{2+} on *L. gibba*. FTIR analyses suggest the involvement of hemicellulose and cellulose in the biosorption of Ni^{2+} and Zn^{2+}. The presence of Ni^{2+} and Zn^{2+} on the *L. gibba* surface was validated by SEM-EDX.

Keywords: competitive biosorption; divalent nickel; divalent zinc; pH and metal concentration effect; *Lemna gibba*; single and binary metal biosorption isotherm

1. Introduction

Soil, surface water, and groundwater pollution by divalent nickel (Ni^{2+}) and zinc (Zn^{2+}) ions can occur by natural processes, but is predominantly due to anthropogenic activities [1], especially the Ni^{2+}- and Zn^{2+}-contaminated discharges from industrial and commercial processes, including mining; mineral processing; electroplating; production of paints, batteries, coins, and electronic commodities; and many other applications [2,3].

Ni^{2+} and Zn^{2+} are essential minerals for some living beings [4]. However, at high concentrations, they are of serious environmental, public health, human well-being, and economic concern due to their toxic effects on cell physiology and metabolism, which can decrease the viability of living organisms or even cause their death [5]. Human exposure to high Ni^{2+} and Zn^{2+} levels has been associated with serious acute and chronic health effects. Ni^{2+} induces hematotoxic, inmunotoxic, hepatotoxic, pulmonary toxic, nephrotoxic, and embryotoxic effects, allergic reactions, and contact dermatitis. In addition, Ni^{2+} impairs the natural balance of essential minerals and is a carcinogenic and

teratogenic agent [6,7]. Zn^{2+} may cause nausea, anemia, vomiting, diarrhea, depression, and lethargy, and circulatory, liver, renal, and neurological disorders [4,8]. Furthermore, it has been reported that the toxicity of binary mixtures of Ni^{2+} and Zn^{2+} is higher than expected from that of individual heavy metals in the mixture. Ni^{2+} and Zn^{2+} exert additive or synergistic negative effects on physiological and biochemical processes of organisms [1,9,10]. Therefore, it is crucial to effectively remove Ni^{2+} and Zn^{2+} ions from industrial and domestic wastewater in order to guarantee that the quality of the treated wastewater meets the recommended standards for its intended use, and to protect aquatic and terrestrial environments and species, human health, welfare, and safety.

Biosorption technology offers potential advantages over traditional methods for the bioremediation of heavy metal-contaminated industrial and domestic wastewater, including an enhanced efficiency for removing heavy metals from diluted or concentrated aqueous solutions, faster removal rates, low operating costs and capital investment, high flexibility, lack of secondary pollution, ease of operation, simplicity of design, and the possibility of recovering the heavy metals and regenerating the biosorbents [11,12]. The competitive advantage of this technology increases when cheap, green, abundant, and widely available biosorbents are used [4].

However, most of the heavy metal biosorption studies have been performed in single metal component systems, and comparatively fewer studies have been conducted in multi-metal component systems. However, wastewater produced by many anthropogenic activities contains several heavy metal ions and other chemical species that may hinder the biosorption process [13,14]. Therefore, studies on the biosorption of heavy metals in multi-element systems are necessary and crucial to understand real systems because these systems resemble more closely the chemical compositions and physicochemical characteristics of industrial effluents than the single-metal systems [13].

Lemna gibba is a free-floating aquatic angiosperm plant. It is a member of the Araceae family and the Lemnoideae subfamily, also known as duckweed. *L. gibba* grows in tropical and temperate zones throughout a wide range of pH, temperature, and nutrient levels [9]. *L. gibba* is found abundantly throughout the year in many freshwater systems, such as lakes, lagoons, ponds, stream pools, slow flowing rivers, and stagnant waters [15–17]. Duckweeds are considered troublesome because they reproduce rapidly, thereby quickly covering the surfaces of water bodies with a dense layer of small plants. This prevents sunlight penetration and oxygen transfer, affecting the photosynthetic and respiratory activities of aquatic organisms [18]. Nevertheless, *L. gibba* is one of the most productive plants on Earth [15,19] and therefore represents a valuable biomass resource for a variety of useful practical applications.

A promising alternative use for this readily available biomass of *L. gibba* is as a biosorbent for removing toxic, inorganic, and organic contaminants from water and wastewaters. This is because the cell wall of Lemnaceae has carbohydrates (cellulose, hemicellulose, etc.), proteins, lipids, lignin, etc., which contain a variety of chemical functional groups, such as carboxyl, hydroxyl, amino, phosphate, sulfate, etc., which can act as binding sites for the biosorption of organic and/or inorganic contaminants [15,20]. Furthermore, *L. gibba* can be used effectively in several biosorption-desorption cycles of contaminants, thereby decreasing process treatment costs [21]. Additionally, *L. gibba* requires minimal processing (washing, drying, grinding), thereby reducing treatment costs. Likewise, *L. gibba* has no economic value; thus, the costs and risks involved in treatment are vastly reduced.

Nevertheless, there is scant information regarding heavy metal biosorption from aqueous solutions by *L. gibba* [15]. Moreover, to the best knowledge of the authors, no information exists regarding the biosorptive removal of Ni^{2+} and Zn^{2+} ions from aqueous solutions in single and binary metal systems by *L. gibba*.

The present work aimed to assess the potential performance of *L. gibba* for the individual and simultaneous biosorption of Ni^{2+} and Zn^{2+} ions, and to model the single and binary equilibrium biosorption of Ni^{2+} and Zn^{2+} of the duckweed. Furthermore, scanning electron microscopy with energy dispersive X-ray spectroscopy (SEM-EDX) and Fourier transform infrared spectroscopy (FTIR) analyses were conducted to confirm the biosorption of Ni^{2+} and Zn^{2+} ions onto *L. gibba*.

2. Materials and Methods

2.1. Ni^{2+} and Zn^{2+} Stock and Test Solutions

Some 40 mM Ni^{2+} and Zn^{2+} stock solutions were produced by accurately weighing the required amount of $NiSO_4 \cdot 6H_2O$ (J.T. Baker®, Monterrey, Mexico; purity >99.1%) or $ZnSO_4 \cdot 7H_2O$ (J.T. Baker®, Monterrey, Mexico; purity >99.9%) and dissolving it in distilled deionized water. For the single and binary metal biosorption experiments, different initial concentrations of each heavy metal ion were obtained by diluting the stock Ni^{2+} and Zn^{2+} solutions.

2.2. Preparation of Biosorbent

L. gibba was harvested in Xochimilco Lake, Mexico City, Mexico. The macrophyte was exhaustively washed with tap and distilled deionized water to completely remove aquatic plants, other than *L. gibba*, dead insects, garbage, and debris. The duckweed samples were then dried at 60 °C until reaching a dry weight constant; thereafter, the macrophyte was ground using a hammer mill, and the obtained powder was sifted through U.S. ASTM sieves to collect the fraction with particle sizes ranging from 0.3 to 0.5 mm, which was employed further in biosorption experiments.

2.3. Proximate Chemical Analysis of Biosorbent

Proximate chemical analysis of *L. gibba* samples was performed in triplicate, following the procedures described in the AOAC handbook [22]. We applied the Soxhlet method to quantify ether extract (*EE*). Total protein (*TP*) was determined using the Kjeldahl method, with 6.25 as the conversion factor from total nitrogen to total protein. Crude fiber (*CF*) was analyzed in terms of the loss in ignition of dried lipid-free residues, following digestion with H_2SO_4 and NaOH standard solutions. Ash (*A*) was verified by burning samples in a muffle furnace at 600 °C, until the weight was constant. Nitrogen-free extract (*NFE*) was quantified as the difference between dry matter and the sum of ash, total protein, ether extract, and crude fiber (Equation (1)):

$$\%NFE = 100 - \%A - \%TP - \%EE - \%CF \quad (1)$$

2.4. Biosorption Studies

Biosorption tests were conducted to examine the effects of metal solution pH and the initial concentrations of Ni^{2+} and Zn^{2+} ions on equilibrium metal biosorption by *L. gibba*. Previous kinetic studies showed that equilibrium times for Ni^{2+} and Zn^{2+} biosorption were less than 48 h (data not shown). Thus, contact time between *L. gibba* and Ni^{2+} or Zn^{2+}, or mixtures of Ni^{2+} and Zn^{2+} solutions, of 48 h was used in equilibrium biosorption studies.

All single and binary equilibrium biosorption tests were conducted in Erlenmeyer flasks (500 mL) containing 1 g (dry weight) L^{-1} of *L. gibba* biomass and 100 mL of metal solution, with a constant agitation (Cole Parmer®, Vernon Hills, IL, USA) of 180 rpm and a temperature of 20 °C.

In the single metal biosorption systems, the effects of the solution pH level on *L. gibba* Ni^{2+} and Zn^{2+} biosorption were explored in metal solutions at 2 mM initial Ni^{2+} or Zn^{2+} concentration, with solution pH values ranging from 1.0 to 6.0. Similar experiments covering the same range of solution pH values were performed to explore the influence of metal solution pH levels on the simultaneous biosorption of Ni^{2+} and Zn^{2+} ions onto *L. gibba*, using an equimolar initial concentration of 2 mM of both heavy metals. Metal solution pH values higher than 6.0 were not assayed to prevent the precipitation of insoluble $Zn(OH)_2$ in the single and binary metal biosorption experiments [23]; 0.1 M NaOH or HCl solutions were used to adjust the pH of each monometal and bimetal solution to the desired value.

To investigate the influences of initial Ni^{2+} or Zn^{2+} concentration on their removal by *L. gibba* in single-metal systems, the initial concentrations of Ni^{2+} or Zn^{2+} ions were varied over the 0.2–30 mM range (0.2, 0.4, 1, 2, 4, 6, 10, 20, and 30 mM). For the two-metal systems, a series of tests were conducted with a constant concentration of the first metal within the interval from 0.2 to 10 mM (0.2, 0.4, 1, 2, 4,

6, and 10 mM), while varying the concentration of the second metal (0.2, 0.4, 1, 2, 4, 6, and 10 mM). A total of 49 different bimetallic systems were assayed combining the two heavy metals studied. In the two-metal systems, no experiments were performed at initial concentrations of each heavy metal greater than 10 mM due to interferences in the quantification of the two metals.

The flasks were taken out from the shaker bath (Cole Parmer®, Vernon Hills, IL, USA) at the end of the batch biosorption experiments, and the biosorbent was separated from the aqueous solutions by filtration (Whatman® grade 42, St. Louis, MI, USA). Filtrates were further used to quantify residual Ni^{2+} and/or Zn^{2+} concentrations.

Control experiments without *L. gibba* biomass were carried out simultaneously using the same conditions as those employed for the Ni^{2+} and/or Zn^{2+} biosorption tests to determine the loss of heavy metal ions by precipitation and/or adsorption onto the glass wall. No statistically significant differences were encountered in the Ni^{2+} and/or Zn^{2+} concentrations of the controls without *L. gibba* biomass, thereby corroborating that the removal of Ni^{2+} and/or Zn^{2+} ions in the experiments using *L. gibba* was caused solely by the macrophyte biosorbent.

The equilibrium Ni^{2+} and Zn^{2+} biosorption capacities (q_e, mmol g^{-1}) were quantified according to the following equation (Equation (2)):

$$q_e = \frac{C_0 - C_e}{M} \tag{2}$$

where C_0 and C_e are the initial and equilibrium Ni^{2+} or Zn^{2+} concentrations of the liquid phase (mmol L^{-1}), respectively; and M is the *L. gibba* concentration (g L^{-1}).

The quantitative simultaneous biosorption effect of both the heavy metals on *L. gibba* was evaluated according to global index of behavior (ξ), and ratio of biosorption capacities (R_q), which were estimated as follows:

$$\xi_{Ni} = 100\frac{\left(\int_{C_{0Ni}=0}^{C_{0Ni}=C_{0Ni}} q_{eNi}dCoNi\right)_b - \left(\int_{C_{0Ni}=0}^{C_{0Ni}=C_{0Ni}} q_{eNi}dCoNi\right)_m}{\left(\int_{C_{0Ni}=0}^{C_{0Ni}=C_{0Ni}} q_{eNi}dCoNi\right)_m} \tag{3}$$

$$\xi_{Zn} = 100\frac{\left(\int_{C_{0Zn}=0}^{C_{0Zn}=C_0Zn} q_{eZn}dCoZn\right)_b - \left(\int_{C_{0Zn}=0}^{C_{0Zn}=C_{0Zn}} q_{eZn}dCoZn\right)_m}{\left(\int_{C_{0Zn}=0}^{C_0Zn=C_{0Zn}} q_{eZn}dCoZn\right)_m} \tag{4}$$

$$R_{qNi} = \frac{q_{eNi,b}}{q_{eNi,m}} \tag{5}$$

$$R_{qZn} = \frac{q_{eZn,b}}{q_{eZn,m}} \tag{6}$$

where ξ_{Ni} and ξ_{Zn} are the global indexes of behavior for Ni^{2+} and Zn^{2+} biosorption at different initial concentrations of Zn^{2+} and Ni^{2+}, respectively; $(q_{eNi}dC_0Ni)_m$ and $(q_{eNi}dC_0Ni)_b$ are the variations of the equilibrium biosorption capacity for Ni^{2+} over initial Ni^{2+} concentration in single and binary metal experiments, respectively; $(q_{eZn}dC_0Zn)_m$ and $(q_{eZn}dC_0Zn)_b$ are the variations of the equilibrium Zn^{2+} biosorption capacity over initial Zn^{2+} concentration in single and binary metal experiments, respectively; $q_{eNi,m}$ and $q_{eZn,m}$ are the equilibrium Ni^{2+} and Zn^{2+} biosorption capacities in the single metal systems respectively; and $q_{eNi,b}$ and $q_{eZn,b}$ are the equilibrium Ni^{2+} and Zn^{2+} biosorption capacities in the binary metal systems, respectively.

The experimental curves represented by $(q_{eNi}dC_0Ni)_m$, $(q_{eNi}dC_0Ni)_b$, $(q_{eZn}dC_0Zn)_m$, and $(q_{eZn}dC_0Zn)_b$ were integrated using scientific and statistical software (GraphPad Prism 8.4, GraphPad Software, San Diego, CA, USA, 2020). $\xi = 0$ indicates that the biosorption of one heavy metal is not affected by the other heavy metal present in the binary metal solution; if $\xi > 0$, that signifies an improvement in the biosorption of a heavy metal in the bimetal system as compared to the monometal system (i.e., positive or synergic effect); and if $\xi < 0$, that denotes a diminution in the biosorption of a

heavy metal in the bimetal system compared to the monometal system (i.e., negative or antagonist effect). Furthermore, R_q = 1.0 indicates that the biosorption of each heavy metal is independent (i.e., non-interaction between Ni^{2+} and Zn^{2+} ions); if $R_q > 1.0$, that indicates that the biosorption of one heavy metal is enhanced by the presence of the other heavy metal (i.e., synergic effect); and if $R_q < 1.0$, it denotes that the biosorption of one heavy metal is suppressed by the other heavy metal present in the metal mixture (i.e., antagonist effect).

2.5. Modeling of Single and Binary Equilibrium Biosorption Isotherms of Ni^{2+} and Zn^{2+} Ions

Modeling experimental equilibrium biosorption isotherm data is an essential tool for trustworthy derivation of design parameters, the comparison of quantitative biosorption performances of distinct biosorption systems, and for diverse conditions in each biosorption system. These equilibrium biosorption isotherm parameters frequently provide some understanding of the affinity and surface characteristics of the biosorbent, in addition to the interactions between the biosorbent and adsorbate, and are consequently required to understand the biosorption mechanism [24]. Therefore, it is critical to establish the most suitable biosorption isotherm model that can be used for optimizing the operation conditions and designing of future large-scale biosorption facilities [24].

2.5.1. Mono-Component Isotherm Models

Equilibrium data for biosorption of single components can be commonly interpreted by the Freundlich, Langmuir, Redlich–Peterson, and Sips isotherms.

Freundlich Isotherm Model

The Freundlich model describes non-ideal, multi-layer biosorption onto heterogeneous surfaces, indicating that biosorption sites are neither independent nor equivalent [25,26]. The Freundlich isotherm model is provided below (Equation (7)):

$$q_e = K_F C_F^{\frac{1}{n_F}} \tag{7}$$

where the Freundlich parameters $1/n_F$ and K_F are relative indicators of intensity and capacity of biosorption, respectively [25].

Langmuir Isotherm Model

This isotherm model has the following assumptions: (1) each biosorption site can adsorb only one molecule of adsorbate, and consequently, only one layer of biosorbed molecules can be formed on the biosorbent surface; (2) there are no interactions between biosorbed species; (3) all the biosorption sites are identical; (4) the capability of a molecule to be biosorbed onto a given biosorption site is not dependent on the occupancy of its neighboring sites; and (5) the biosorptive forces are similar to those found in chemical interactions [26,27]. The Langmuir equation can be expressed as follows (Equation (8)):

$$q_e = \frac{q_{max} B_L C_e}{1 + B_L C_e} \tag{8}$$

where q_{max} is the theoretical maximum biosorption capacity of the biosorbent; q_e is the biosorption capacity at the equilibrium; C_e is the equilibrium adsorbate concentration in the liquid phase; and B_L is the Langmuir constant that represents the reciprocal of the adsorbate concentration at which half saturation of the biosorbent is reached [25].

Sips Isotherm Model

The Sips equation is a hybrid model of the Freundlich and Langmuir isotherms, used extensively to interpret equilibrium biosorption data. It has the following form (Equation (9)) [28]:

$$q_e = \frac{q_{max} B_S C_e{}^{n_S}}{1 + (B_S C_e{}^{n_S})} \quad (9)$$

where q_{max} is the maximum biosorption capacity; B_s is the Sips constant; and n_s is the Sips parameter that characterizes the system's heterogeneity.

Redlich–Peterson Isotherm Model

The Redlich–Peterson isotherm equation is shown in Equation (10) [27]:

$$q_e = \frac{K_{RP} C_e}{1 + (A_{RP} C_e{}^{b_{RP}})}, \; 0 \le b_{RP} \le 1 \quad (10)$$

where K_{RP}, A_{RP}, and b_{RP} are the model parameters. This model reduces to the Langmuir isotherm when $b_{RP} = 1$, to the Freundlich isotherm at high concentration of the adsorbate, and to a linear isotherm at low surface coverage.

2.5.2. Multi-Component Isotherm Models

In the case of binary metal or multi-metal systems, as is representative of industrial wastewaters, there may be interference and competition between different components for biosorption binding sites, resulting in a more complex mathematical description of the dynamic equilibrium state [29]. Therefore, the isotherm models proposed for single-component biosorption equilibrium have been modified and extended to represent the binary component and multi-component biosorption equilibria over a wide range of solution concentrations [30]. However, despite its great significance for the design of treatment systems, the equilibrium modeling of binary component and multi-component biosorption has largely been neglected [29].

Seven different multi-component isotherm models were applied to describe the simultaneous biosorption of Ni^{2+} and Zn^{2+} ions onto *L. gibba*, namely, non-modified competitive Langmuir, modified competitive Langmuir, modified Langmuir with an interaction factor, extended Freundlich, non-modified competitive Redlich–Peterson, modified Redlich–Peterson with interaction factor, and modified Sips isotherm models.

Non-Modified Competitive Langmuir Isotherm Model

This model has the same assumptions as the monocomponent Langmuir isotherm equation and can be expressed for components Ni^{2+} and Zn^{2+} in a mixture of both heavy metals as follows [31]:

$$q_{eNi} = \frac{q_{maxNi} B_{Ni} C_{eNi}}{1 + B_{Ni} C_{eNi} + B_{Zn} C_{eZn}} \quad (11)$$

$$q_{eZn} = \frac{q_{maxZn} B_{Zn} C_{eZn}}{1 + B_{Ni} C_{eNi} + B_{Zn} C_{eZn}} \quad (12)$$

where q_{eNi} and q_{eZn} are the equilibrium biosorption capacities of Ni^{2+} and Zn^{2+} in the bimetal system; C_{eNi} and C_{eZn} are the equilibrium Ni^{2+} and Zn^{2+} concentrations in binary metal solution; B_{Ni} and B_{Zn} are the constants of the Langmuir model for Ni^{2+} and Zn^{2+} biosorption in monometal systems; and q_{maxNi} and q_{maxZn} are the theoretical maximum biosorption capacities of Ni^{2+} and Zn^{2+} in the single metal systems, respectively [32].

Modified Competitive Langmuir Isotherm

Assuming the active biosorption sites are distributed uniformly on the biosorbent surface, and all the adsorbates in the liquid phase compete for the same biosorption sites of the biosorbent, the Langmuir model for single-component systems was extended for multicomponent systems as follows [30]:

$$q_{eNi} = \frac{q_{maxNi}{}' B_{Ni}{}' \, C_{eNi}}{1 + B_{Ni}{}' C_{eNi} + B_{Zn}{}' C_{eZn}} \tag{13}$$

$$q_{eZn} = \frac{q_{maxZn}{}' B_{Zn}{}' C_{eZn}}{1 + B_{Ni}{}' C_{eNi} + B_{Zn}{}' C_{eZn}} \tag{14}$$

The parameters $q_{maxNi}{}'$, $q_{maxZn}{}'$, $B_{Ni}{}'$, and $B_{Zn}{}'$ can be obtained from the fitting of Equations (13) and (14) with the experimental equilibrium biosorption data of Ni^{2+} and Zn^{2+} in the binary metal system [30].

Modified Langmuir Isotherm with an Interaction Factor η

In multicomponent biosorption systems, the biosorbent affinity for the adsorbates changes due to biosorbent-adsorbate interactions and the competition of the heavy metal ions species for biosorption binding sites. Considering these effects, an interaction term (η) for each adsorbate has been introduced into Equations (11) and (12) to yield Equations (15) and (16) [31].

$$q_{eNi} = \frac{q_{maxNi} B_{Ni} \frac{C_{eNi}}{\eta_{Ni}}}{1 + B_{Ni} \frac{C_{eNi}}{\eta_{Ni}} + B_{Zn} \frac{C_{eZn}}{\eta_{Zn}}} \tag{15}$$

$$q_{eZn} = \frac{q_{maxZn} B_{Zn} \frac{C_{eZn}}{\eta_{Zn}}}{1 + B_{Ni} \frac{C_{eNi}}{\eta_{Ni}} + B_{Zn} \frac{C_{eZn}}{\eta_{Zn}}} \tag{16}$$

where η_{Ni} and η_{Zn} are characteristic of Ni^{2+} and Zn^{2+} ions and dependent on the concentrations of the other components in the solution [30]. These characteristic parameters can be obtained from the experimental competitive biosorption data of Ni^{2+} and Zn^{2+} ions.

Extended Freundlich Isotherm

The single-component Freundlich equation has been extended to represent the binary component biosorption system, and is expressed according to Equations (17) and (18) for each heavy metal of the binary mixture of adsorbates [30]:

$$q_{eNi} = \frac{K_{FNi} C_{eNi}^{\frac{1}{n_{FNi}} + x_{Ni}}}{C_{eNi}{}^{x_{Ni}} + y_{Ni} C_{eZn}{}^{z_{Ni}}} \tag{17}$$

$$q_{eZn} = \frac{K_{FZn} C_{NZn}^{\frac{1}{n_{FZn}} + x_{Zn}}}{C_{eZn}{}^{x_{Zn}} + y_{Zn} C_{eNi}{}^{z_{Zn}}} \tag{18}$$

where K_{FNi}, K_{FZn}, n_{FNi}, and n_{FZn} are Freundlich parameters that are obtained from the corresponding single-component Freundlich isotherm models; whereas x_{Ni}, y_{Ni}, z_{Ni}, and x_{Zn}, y_{Zn}, and z_{Zn} are the competitive Freundlich biosorption parameters for Ni^{2+} and Zn^{2+} ions, respectively.

Modified Sips Isotherm

The single-component Sips isotherm model can be extended to describe the biosorption in binary-component systems [32]:

$$q_{eNi} = \frac{q_{maxNi} B_{sNi} C_{eNi}{}^{n_{sNi}}}{1 + B_{sNi} C_{eNi}{}^{n_{sNi}} + B_{sZn} C_{eZn}{}^{n_{sZn}}} \tag{19}$$

$$q_{eZn} = \frac{q_{maxZn} B_{sZn} C_{eZn}{}^{n_{sZn}}}{1 + B_{sNi} C_{eNi}{}^{n_{sNi}} + B_{sZn} C_{eZn}{}^{n_{sZn}}} \quad (20)$$

where the modified Sips model parameters q_{maxNi}, q_{maxZn}, B_{sNi}, B_{sZn}, n_{sNi}, and n_{sZn} are obtained from binary component biosorption data [32].

Non-Modified Competitive Redlich-Peterson Isotherm

The competitive Redlich–Peterson isotherm models for binary component biosorption systems are given in Equations (21) and (22):

$$q_{eNi} = \frac{K_{RPNi} C_{eNi}}{1 + A_{RPNi} C_{eNi}{}^{b_{RPNi}} + A_{RPZn} C_{eZn}{}^{b_{RPZn}}} \quad (21)$$

$$q_{eZn} = \frac{K_{RPZn} C_{eZn}}{1 + A_{RPNi} C_{eNi}{}^{b_{RPNi}} + A_{RPZn} C_{eZn}{}^{b_{RPZn}}} \quad (22)$$

where K_{RPNi}, K_{RPZn}, A_{RPNi}, A_{RPZn}, b_{RPNi}, and b_{RPZn} are the single-component Redlich–Peterson model parameters for the Ni^{2+} and Zn^{2+} ions components [33].

Modified Redlich-Peterson Isotherm with Interaction Factor η

The competitive Redlich–Peterson isotherm model can be extended with an interaction factor η, in a manner analogous to that of the modified Langmuir isotherm model, and can be expressed for components Ni^{2+} and Zn^{2+} in a bimetal system [34] as follows:

$$q_{eNi} = \frac{K_{RPNi} \frac{C_{eNi}}{\eta_{Ni}}}{1 + A_{RPNi} \left(\frac{C_{eNi}}{\eta_{Ni}} \right)^{b_{RPNi}} + A_{RPZn} \left(\frac{C_{eZn}}{\eta_{Zn}} \right)^{b_{RPZn}}} \quad (23)$$

$$q_{eZn} = \frac{K_{RPZn} \frac{C_{eZn}}{\eta_{Zn}}}{1 + A_{RPNi} \left(\frac{C_{eNi}}{\eta_{Ni}} \right)^{b_{RPNi}} + A_{RPZn} \left(\frac{C_{eZn}}{\eta_{Zn}} \right)^{b_{RPZn}}} \quad (24)$$

where η_{Ni} and η_{Zn} are the correction coefficients for Ni^{2+} and Zn^{2+} ions estimated from binary metal biosorption data; and K_{RPNi}, K_{RPZn}, A_{RPNi}, A_{RPZn}, b_{RPNi}, and b_{RPZN} are derived from the corresponding single-component biosorption data [34].

2.6. Determination of Isotherm Parameters and Statistical Analysis

Batch biosorption experiments were conducted in triplicate to confirm the reproducibility of the results and for statistical analysis. The data reported herein represent the mean values ± standard deviations. Biosorption data of Ni^{2+} and Zn^{2+} were analyzed by variance analysis and Tukey's test ($p < 0.05$), using GraphPad Prism 8.4 (GraphPad Software, San Diego, CA, USA, 2020).

The isotherm parameters of all the single-metal and binary-metal models were obtained by nonlinear regression analysis using the software MATLAB® (version 2020a; The Mathworks, Inc., Natick, MA, USA, 2020). The standard deviation of the residuals (*RMSE* and *Sy.x*), the sum of squares error (*SSE*), and the coefficient of determination (R^2) were used to determine the adequacy and accuracy of the fit of the various isotherm models assayed with the experimental data. Small *RMSE*, *Sy.x*, *SSE* values, and a value of R^2 near 1.0 indicate a better description of experimental biosorption data by a particular model [28].

2.7. FTIR Analysis

FTIR spectroscopy was employed to gain information about the main chemical functional groups present on the *L. gibba* surface, and to detect possible modifications of active biosorption sites on the *L. gibba* surface during the biosorption of Ni^{2+}, Zn^{2+}, or the binary mixture of Ni^{2+} and Zn^{2+} ions.

L. gibba (1 g L^{-1}) samples were mixed with aqueous solutions of 10 mM Ni^{2+}, 10 mM Zn^{2+}, or with 10 mM solutions of equimolar mixtures of Ni^{2+} and Zn^{2+} ions at pH 6.0 ± 0.1 for 24 h, with constant agitation at 180 rpm and 20 ± 1 °C to saturate the active biosorption sites with Ni^{2+}, Zn^{2+}, or with both Ni^{2+} and Zn^{2+} ions. The resulting suspensions were subsequently centrifuged for 5 min at 5000 rpm to pellet the *L. gibba* biomass. The pellets collected were washed thoroughly with distilled deionized water to remove the unbound heavy metals. After centrifuging the resulting suspensions, the obtained heavy metal-loaded *L. gibba* biomass was dried at 105 °C to remove any retained water which could interfere with the detection of hydroxyl functional groups on the *L. gibba* surface [35].

Finely ground raw (i.e., not loaded with Ni^{2+} and/or Zn^{2+} ions) and heavy metal-loaded *L. gibba* samples were mixed with dried potassium bromide (Merck™, Germany; spectroscopic grade) in a ratio of 1:5 and examined by diffuse reflectance FTIR spectroscopy in a Perkin–Elmer FTIR spectrophotometer (Spectrum 2000, Perkin-Elmer, Inc., Waltham, MA, USA). FTIR spectra data were collected over the wavenumber range of 4000–400 cm^{-1}, at a resolution of 4 cm^{-1}, for a total of 16 scans.

2.8. SEM and SEM-EDX Analysis

The surface structures of *L. gibba* samples, prior to and following saturation with Ni^{2+} and/or Zn^{2+} ions, were studied using a scanning electron microscope (SEM; FEI Quanta Dual Beam Instrument, FEI Company, Hillsboro, OR, USA) with an accelerated voltage of 15 kV. The analysis of chemical elements was conducted by energy dispersive X-ray spectrometry (EDX) using an Apollo X detector (EDAX, AMETEK, Inc., Berwyn, PA, USA). For the analysis, samples remained uncoated at low vacuum conditions to improve electron conductivity and image quality.

2.9. Analytical Techniques

Ni^{2+} and Zn^{2+} concentrations in liquid solution were assessed colorimetrically using a UV-Vis Evolution 201 (Thermo Fisher Scientific, Whaltman, MA, USA) spectrophotometer, following the methodology outlined in the Hach Water Analysis Handbook [36]. Ni^{2+} and Zn^{2+} concentrations were determined from calibration curves established for each heavy metal with a minimum of seven concentration levels.

3. Results and Discussion

3.1. Proximate Composition of L. gibba

The analysis results of the proximate chemical composition of *L. gibba* are as follows (on a dry matter basis): total carbohydrates, 46.57 ± 1.5%; total proteins, 26.29 ± 0.51%; total ashes, 19.04 ± 0.41%; and total lipids, 8.10 ± 0.05%. It is apparent that *L. gibba* is rich in carbohydrates and proteins and has a low fat content. These findings concur with those reported for the Lemnaceae by Schmid and Landolt [37] and Landesman [38]. The polymeric compounds present in *L. gibba* biomass have many chemical functional groups that can be binding sites for the biosorptive removal of toxic metal ions from aqueous solutions.

3.2. Influences of Metal Solution pH on the Individual and Simultaneous Biosorption of Ni^{2+} and Zn^{2+} onto L. gibba

The pH of a metal ion solution is among the crucial environmental factors that affect heavy metal biosorption from liquid solutions due to its ability to influence the chemical speciation, degree of ionization, and aqueous solubility of heavy metals. Metal ion solution pH also influences competition

with other heavy metal ions present in the liquid phase and the dissociation degree of chemical functional groups present on the surface of biosorbents [11,12].

To find the optimum value of solution pH for Ni^{2+} and Zn^{2+} biosorption onto *L. gibba* for the single metal and binary metal systems, biosorption tests with the solution pH varying from 1.0 to 6.0 were performed. The influences of the pH of the aqueous metal solution on the equilibrium Ni^{2+} and Zn^{2+} biosorption capacities for the single and binary heavy metal systems are illustrated in Figure 1.

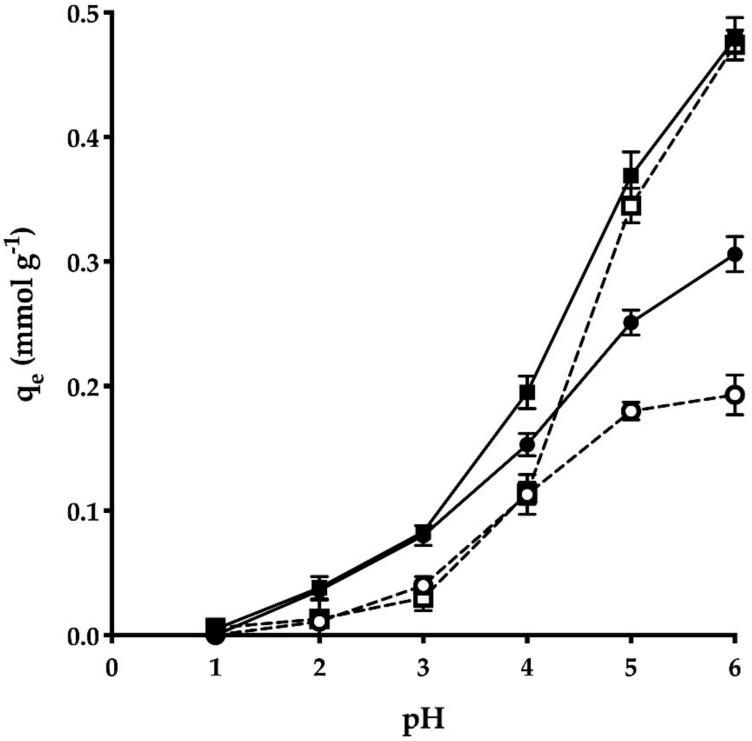

Figure 1. The effects of solution pH on Ni^{2+} and Zn^{2+} biosorption from aqueous solutions by *Lemna gibba* in single (●— Ni^{2+}, —■— Zn^{2+}) and binary (---○--- Ni^{2+}, ---□--- Zn^{2+}) metal systems.

It is apparent that the equilibrium biosorption capacities of Ni^{2+} and Zn^{2+} ions increased as the solution pH increased and reached its highest value at pH 6.0, both for the mono-metal and bi-metal systems. This biosorption behavior may be due to the fact that at low solution pH levels, the active binding sites available on the *L. gibba* surface are mostly protonated, resulting in electrostatic repulsion between the Ni^{2+} and Zn^{2+} cationic species and the positive electrical surface charges of *L. gibba*, and the competition between H^+ ions and Ni^{2+} and Zn^{2+} ions for occupancy of the binding sites. Contrastingly, the extent of Ni^{2+} and Zn^{2+} biosorption increases with increasing solution pH presumably due to a decrease in competition between H^+ ions and Ni^{2+} and Zn^{2+} ions for the biosorption binding sites, and also due to an increase in the number of negative electrical charges on the *L. gibba* surface, which results in a greater electrostatic attraction between the *L. gibba* surface and Ni^{2+} and Zn^{2+} ions [11].

Previous studies have reported an optimal solution pH of 6.0 for Ni^{2+} and Zn^{2+} biosorption in single metal systems [39–41]. However, to the best knowledge of the authors, no works have investigated the influence of pH of the metal solution on the simultaneous biosorption of Ni^{2+} and Zn^{2+} ions from an aqueous solution.

The capacities of Zn^{2+} biosorption were higher than those of Ni^{2+} at pH values greater than 3.0 and 4.0, for the single metal and binary metal systems, respectively. At solution pH values of 5.0 and 6.0, no statistically significant difference was observed in Zn^{2+} biosorption capacities between single and binary metal systems, which indicates that Zn^{2+} biosorption onto *L. gibba* was not significantly

affected by the presence of Ni^{2+} ions at the studied conditions. Contrastingly, a noticeable decrease in biosorption capacity of Ni^{2+} was observed when Zn^{2+} ions were present in the metal solution with pH values between 3.0 and 6.0.

The results show that the solution pH of 6.0 is most suitable for the single and binary Ni^{2+} and Zn^{2+} biosorption onto *L. gibba*. Consequently, all subsequent experiments were conducted with a solution pH of 6.0.

3.3. Influence of Initial Metal Concentration in the Single and Binary Biosorption Systems of Ni^{2+} and Zn^{2+} onto L. gibba

The influences of initial concentrations of Ni^{2+} and Zn^{2+} on the *L. gibba* equilibrium biosorption capacities of the heavy metals in monometal and bimetal systems are displayed in Figures 2 and 3, respectively. The capacity of metal biosorption of *L. gibba* increased as the initial concentration of Ni^{2+} or Zn^{2+} in single (Figure 2) and binary metal systems increased (Figure 3).

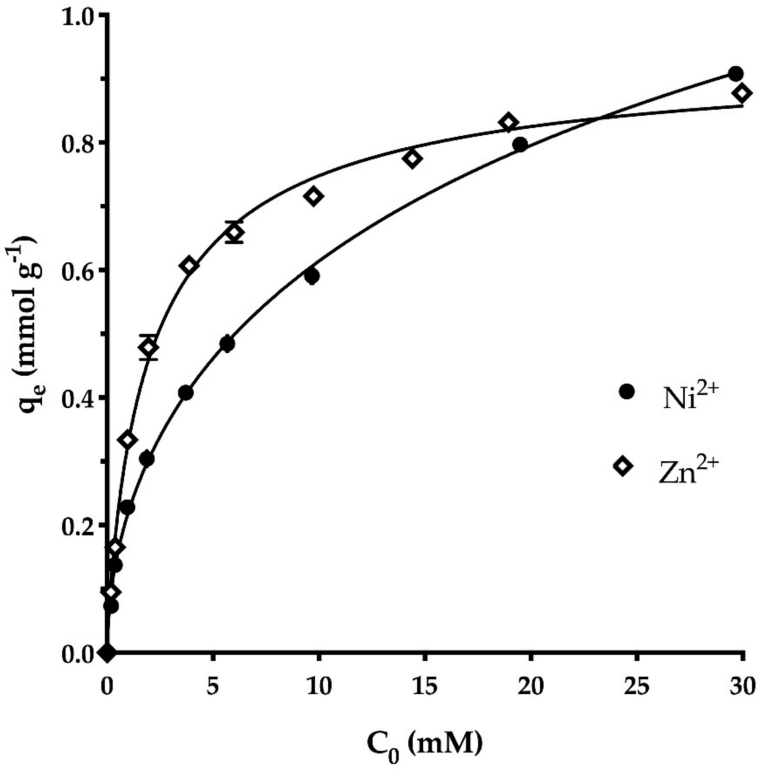

Figure 2. The effects of initial metal concentration on Ni^{2+} and Zn^{2+} biosorption from aqueous solutions in single metal systems.

These results can be attributed to the fact that the greater the initial concentration of Ni^{2+} or Zn^{2+} ions, the greater the number of Ni^{2+} or Zn^{2+} ions in the aqueous metal solution, which results in a greater number of interactions between the metal ions and the *L. gibba* biomass. Additionally, a higher initial Ni^{2+} or Zn^{2+} concentration also causes metal concentration gradient increases, resulting in a faster transfer of Ni^{2+} or Zn^{2+} ions from the bulk of the liquid phase to the *L. gibba* surface due to an enhanced mass transfer coefficient, along with providing the driving force to overwhelm the mass transfer resistances of Ni^{2+} or Zn^{2+} ions between the liquid phase and the *L. gibba* biomass [11,12].

Figure 2 shows that *L. gibba*'s Zn^{2+} biosorption capacity was higher than Ni^{2+} biosorption capacity up to a 15 mM initial metal concentration in the single metal systems. At higher initial metal concentrations, the Ni^{2+} and Zn^{2+} biosorption capacities were similar. However, the initial slope of the curve that relates Zn^{2+} biosorption capacity as a function of initial Zn^{2+} concentration was higher than

the initial slope of the curve relating biosorption capacity of Ni^{2+} ions to initial Ni^{2+} concentration (Figure 2), which indicates that *L. gibba* biomass has a greater affinity for Zn^{2+} ions than for Ni^{2+} ions.

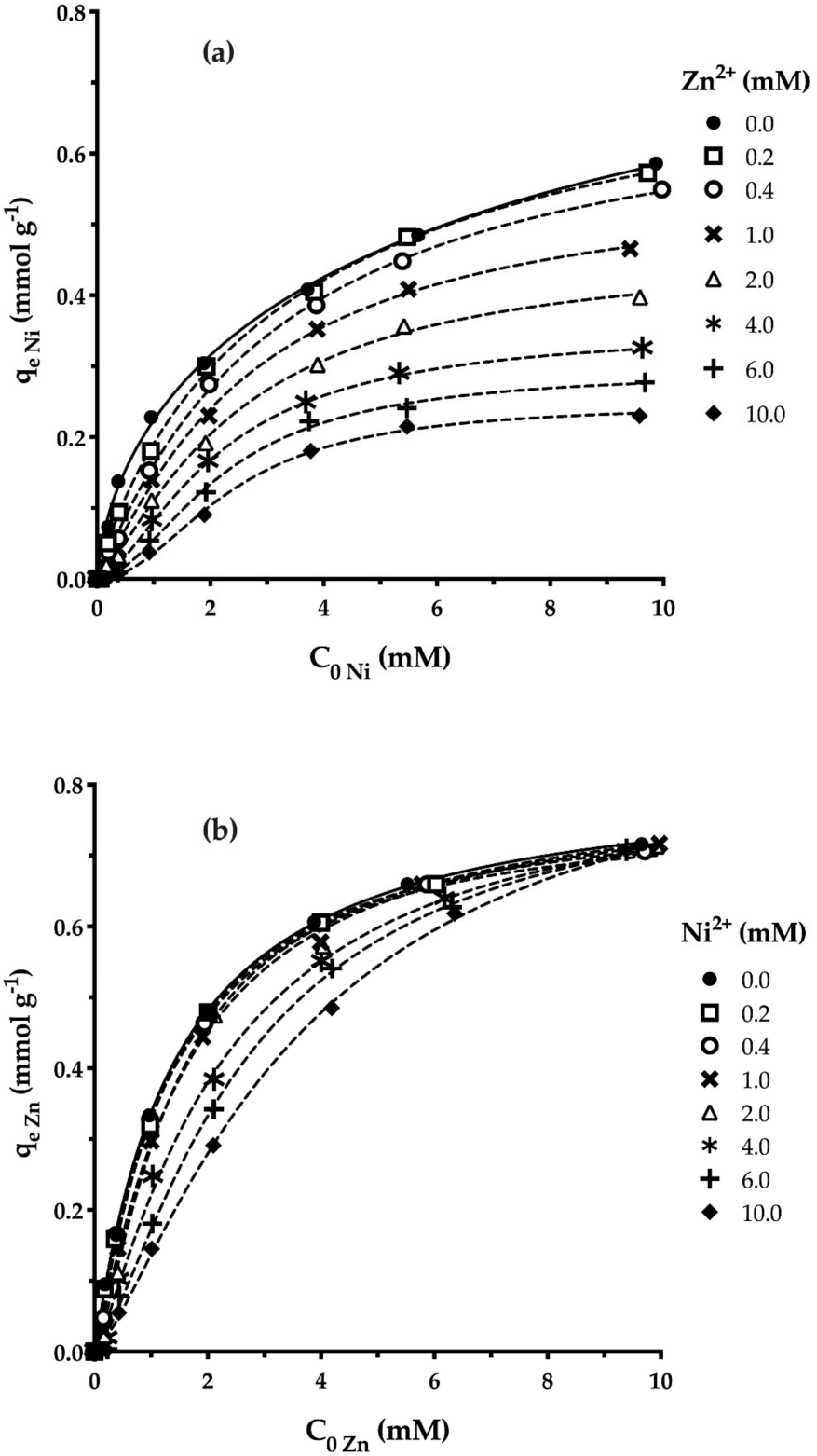

Figure 3. The effects of initial metal concentration on Ni^{2+} (**a**) and Zn^{2+} (**b**) biosorption from aqueous solutions in binary metal systems.

Similarly, the results of simultaneous biosorption of Ni^{2+} and Zn^{2+} ions also show that the biosorption of a heavy metal was affected to a differing extent by the other heavy metal present in the metal solution, and that *L. gibba* biosorption capacity for Zn^{2+} ions was higher than that for Ni^{2+} ions (Figure 3).

Regardless of the initial concentration of Ni^{2+} assayed, the *L. gibba* Ni^{2+} biosorption capacity at equilibrium decreased with the increasing of initial Zn^{2+} concentration (Figure 3a). Similarly, the global behavior index for the biosorption of Ni^{2+} ions decreased from −2.1% to −60.3% as the initial concentration of Zn^{2+} ions increased from 0.2 to 10 mM (Table 1). This indicates that the greater the initial Zn^{2+} concentration, the higher the adverse effect on Ni^{2+} biosorption.

Table 1. The global index of behavior for Ni^{2+} biosorption (ξ_{Ni}) at different initial Zn^{2+} concentrations.

Initial Zn^{2+} Concentration (mM)	ξ_{Ni} (%)
0.2	−2.096
0.4	−8.474
1	−19.157
2	−30.772
4	−43.319
6	−52.371
10	−60.335

Furthermore, Table 2 displays that R_{qNi} values are far less than 1.0 at almost all initial Zn(II) concentrations, indicating that Zn^{2+} interfered with Ni^{2+} biosorption onto *L. gibba*. These results show that Zn^{2+} inhibited biosorption of Ni^{2+} ions.

Table 2. The ratio of Ni^{2+} biosorption capacity (R_{qNi}) at different initial Zn^{2+} concentrations.

C_{0Zn} (mM)	C_{0Ni} (mM)						
	0.2	**0.4**	**1**	**2**	**4**	**6**	**10**
0.2	0.69	0.68	0.79	0.98	0.99	0.99	0.98
0.4	0.52	0.42	0.67	0.90	0.95	0.92	0.94
1	0.43	0.31	0.61	0.76	0.86	0.84	0.79
2	0.26	0.24	0.49	0.63	0.74	0.74	0.68
4	0.12	0.10	0.36	0.54	0.61	0.59	0.55
6	0.02	0.07	0.24	0.40	0.55	0.50	0.47
10	0.01	0.05	0.16	0.30	0.44	0.44	0.39

C_{0Ni} = Initial Ni^{2+} concentration; C_{0Zn} = Initial Zn^{2+} concentration.

Similarly, Figure 3b and global behavior index data (Table 3) of Zn^{2+} biosorption in the presence of Ni^{2+} ions revealed that the initial concentrations of Ni^{2+} in the range of 0.2 to 2.0 mM have a far lower adverse effect on Zn^{2+} biosorption onto *L. gibba* than initial Ni^{2+} concentrations higher than 2.0 mM.

Table 3. The global index of behavior for Zn^{2+} biosorption (ξ_{Zn}) at different initial Ni^{2+} concentrations.

Initial Ni^{2+} Concentration (mM)	ξ_{Zn} (%)
0.2	−0.127
0.4	−0.374
1	−2.171
2	−2.507
4	−8.548
6	−12.079
10	−16.536

Furthermore, the inhibitory influence of Ni^{2+} on Zn^{2+} biosorption was only evident when the initial concentration of Ni^{2+} was greater than the equimolar ratio (Table 4).

Table 4. The ratio of Zn^{2+} biosorption capacity (R_{qZn}) at different initial Ni^{2+} concentrations.

C_{0Ni} (mM)	C_{0Zn} (mM)						
	0.2	**0.4**	**1**	**2**	**4**	**6**	**10**
0.2	0.93	0.96	0.96	1.00	1.00	1.00	1.00
0.4	0.50	1.00	0.98	0.97	1.00	1.00	0.99
1	0.32	0.88	0.96	0.98	0.95	1.00	1.00
2	0.24	0.68	0.94	0.99	0.94	1.00	1.00
4	0.19	0.61	0.74	0.80	0.91	0.97	0.99
6	0.04	0.48	0.54	0.71	0.89	0.95	1.00
10	0.02	0.33	0.44	0.61	0.80	0.94	1.00

C_{0Ni} = Initial Ni^{2+} concentration; C_{0Zn} = initial Zn^{2+} concentration.

Hence, these results confirm that *L. gibba* biomass has a higher preference for Zn^{2+} ions than for Ni^{2+} ions, and that Zn^{2+} biosorption was almost free from interferences from Ni^{2+} ions at concentration ratios lower than or equal to the equimolar ratio, at the reported working conditions.

The higher biosorption preference of *L. gibba* for Zn^{2+} ions over Ni^{2+} ions could be attributed to the higher ionic radius (Zn, 74 pm; Ni, 69 pm) and atomic weight (Zn, 65.4; Ni, 58.7) of Zn^{2+} than of Ni^{2+}. Generally, the higher the ionic size and atomic weight of a heavy metal, the higher the affinity of a biosorbent for the heavy metal [42,43]. Consequently, the preference of a biosorbent for biosorbing the heavy metal will be maximum [44]. This may be due to the fact that the motion of a heavy metal has a greater atomic mass generating a greater energy of momentum, which can facilitate the binding of the heavy metal to the biosorbent by increasing the probability of interaction between the binding sites of the biosorbent and the heavy metal, leading to a higher biosorption preference by a biosorbent [44].

A higher affinity for the biosorption of Zn^{2+} ions than for Ni^{2+} ions has been previously reported [45].

3.4. Isotherms and Their Modeling

3.4.1. Single-Metal Biosorption Systems

The equilibrium biosorption isotherm provides important information on the interactions between the biosorbent and the adsorbate (e.g., heavy metal) and is consequently needed to understand the mechanism of biosorption [25]. Figure 4 presents the experimental biosorption isotherm of Ni^{2+} (Figure 4a) and Zn^{2+} (Figure 4b) ions at pH 6.0 and at 20 °C, for the single metal systems.

It is evident that the biosorption capacities at the equilibrium of Ni^{2+} and Zn^{2+} increased as the equilibrium concentrations of Ni^{2+} and Zn^{2+} ions in the solution increased. The initial slopes of the Ni^{2+} and Zn^{2+} biosorption isotherms steadily decrease with increasing equilibrium metal concentrations because metal ions have more difficulty finding vacant active biosorption sites with the progressive covering of the *L. gibba* surface. This dynamic indicates a progressive occupation of *L. gibba's* active sites by Ni^{2+} or Zn^{2+} ions [11]. In addition, the initial slope of the Zn^{2+} isotherm was steeper than that of the Ni^{2+} isotherm, which is indicative of a higher affinity of *L. gibba* biomass for Zn^{2+} ions than for Ni^{2+} ions.

Furthermore, the analysis of biosorption equilibrium data is essential to establish the most suitable isotherm equation that characterizes precisely the process of biosorption, which can also be employed to optimize the design and operating conditions of a biosorption system [11,25].

Isotherm models with two (Freundlich and Langmuir) and three (Redlich–Peterson and Sips) parameters were assessed for their ability to fit the experimental data of Ni^{2+} and Zn^{2+} equilibrium biosorption onto *L. gibba*. The biosorption parameters for each metal ion obtained from the non-linear regression analysis of the isotherm models employed in this work are shown in Table 5, together with

the values of R^2, *Sy.x*, *RMSE*, and *SSE*. Likewise, Figure 4 displays the isotherm curves predicted by the four isotherm models.

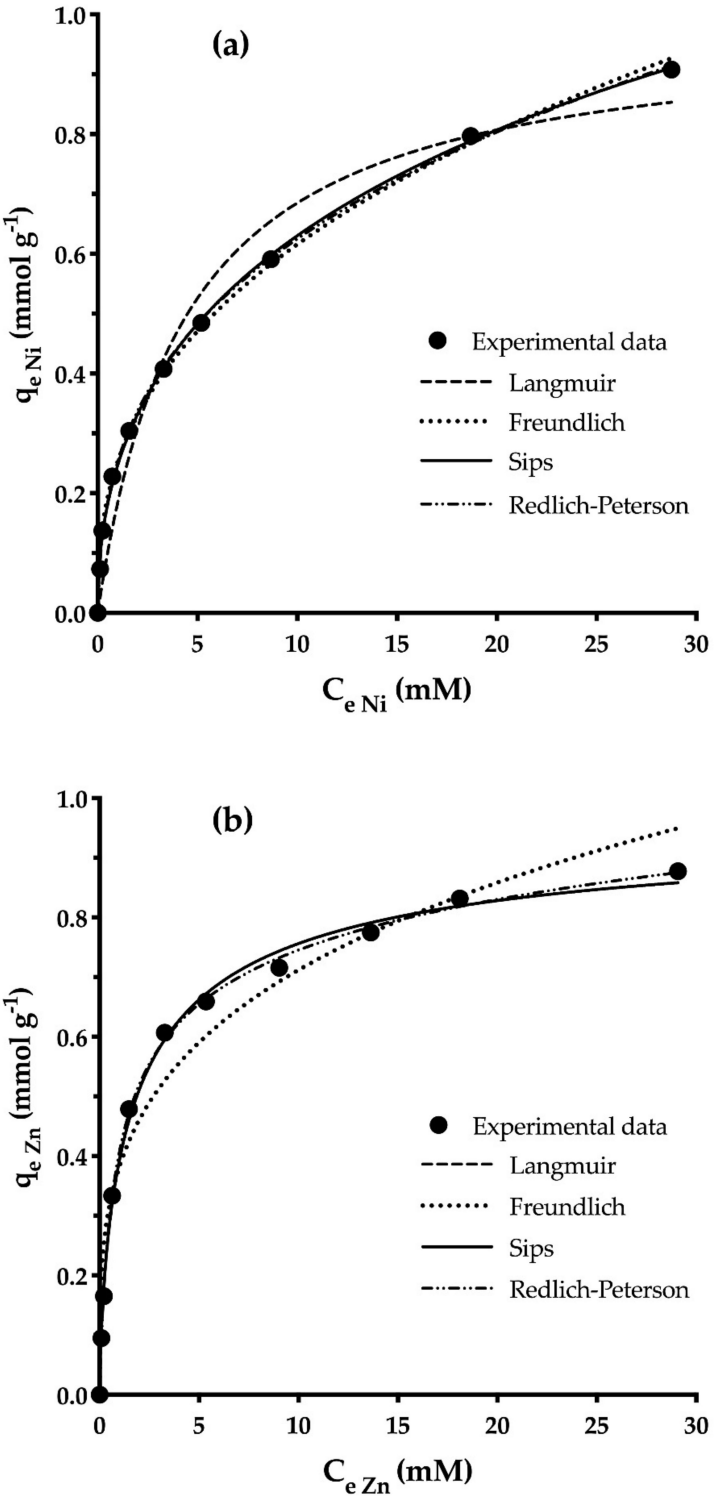

Figure 4. Isotherms of Ni^{2+} (**a**) and Zn^{2+} (**b**) biosorption on *Lemna gibba* in single metal systems.

The Freundlich, Redlich-Peterson, and Sips isotherm equations best described Ni^{2+} biosorption data, as evidenced by the lowest *Sy.x*, *RMSE*, and *SSE* and the highest R^2 values of these models. Nonetheless, the Sips model was not capable of predicting the experimental maximum Ni^{2+} biosorption capacity (q_{max} = 0.91 mmol g^{-1}). Therefore, the Sips model is unsuitable for interpreting the experimental

equilibrium isotherm for the biosorption of Ni^{2+} ions onto *L. gibba*. The Freundlich model parameter n_F, which is related to the biosorption intensity, was found to be 2.59. This value is within the range of 1 to 10, which suggests that Ni^{2+} biosorption by *L. gibba* is favorable at the conditions being studied [11].

Table 5. Isotherm model parameters for Ni^{2+} and Zn^{2+} biosorption in single metal systems.

Model	Ni^{2+}	Zn^{2+}
Langmuir		
q_{max} (mmol g^{-1})	0.982 ± 0.074	0.852 ± 0.022
B_L (L $mmol^{-1}$)	0.231 ± 0.053	0.875 ± 0.112
R^2	0.965	0.9885
SSE	0.029	0.011
Sy.x	0.060	0.0352
RMSE	0.057	0.0333
Freundlich		
K_F (mmol g^{-1}) (mmol L^{-1})$^{-1/nF}$	0.253 ± 0.007	0.382 ± 0.028
n_F	2.587 ± 0.069	3.705 ± 0.388
R^2	0.997	0.961
SSE	0.002	0.037
Sy.x	0.017	0.064
RMSE	0.016	0.061
Sips		
q_{max} (mmol g^{-1})	2.849 ± 0.744	0.974 ± 0.040
B_s (mmol L^{-1})$^{-nS}$	0.095 ± 0.026	0.677 ± 0.061
n_S	0.476 ± 0.03	0.710 ± 0.051
R^2	0.999	0.997
SSE	0.001	0.003
Sy.x	0.011	0.019
RMSE	0.010	0.017
Redlich–Peterson		
K_{RP} (L g^{-1})	1.886 ± 0.523	1.234 ± 0.098
A_{RP} (mmol L^{-1})$^{-BRP}$	6.456 ± 2.038	2.028 ± 0.222
b_{RP}	0.655 ± 0.012	0.885 ± 0.011
R^2	0.999	0.999
SSE	0.001	0.001
Sy.x	0.010	0.011
RMSE	0.009	0.010

Furthermore, according to the error function (R^2, *RMSE*, *Sy.x*, and *SSE*) values, the Langmuir, Redlich–Peterson, and Sips isotherm equations better represented the experimental equilibrium data of Zn^{2+} biosorption onto *L. gibba* than the Freundlich model. However, the Sips model was unable to adequately predict the maximum equilibrium Zn^{2+} biosorption capacity obtained experimentally (0.88 mmol g^{-1}). Thus, the Sips model is not appropriate for describing the biosorption isotherm of Zn^{2+} ions onto *L. gibba*. Contrastingly, the Langmuir model predicted a maximum biosorption capacity of Zn^{2+} ions of 0.852 mmol g^{-1}, which closely matched the experimental value. Similarly, the exponent value of the Redlich–Peterson (b_{RP} = 0.885) model was close to 1.0. In this case, the Redlich–Peterson model is transformed to the Langmuir equation [28].

Considering these results, it is concluded that the Freundlich and Redlich–Peterson models provided the most suitable representations of the biosorption isotherm of Ni^{2+} ions by *L. gibba*, whereas the Langmuir and Redlich–Peterson models best described the equilibrium biosorption pattern for Zn^{2+} biosorption.

Furthermore, the values of the constants B_L of Langmuir equation and n_F of Freundlich equation for Zn^{2+} biosorption are higher than those for Ni^{2+} biosorption. These results confirm that *L. gibba* has a greater affinity for Zn^{2+} ions than for Ni^{2+} ions, as the higher the values of B_L and n_F, the higher the affinity between the adsorbate and biosorbent [30,40].

3.4.2. Binary-Metal Biosorption Systems

For the purpose of representing the equilibrium data of binary biosorption of Ni^{2+} and Zn^{2+} on *L. gibba* in a suitable graphical method, three-dimensional biosorption surfaces were built, plotting the capacity of Ni^{2+} or Zn^{2+} biosorption at equilibrium (*z*-axis) versus the Ni^{2+} and Zn^{2+} concentrations at equilibrium (x- and *y*-axis). Figure 5 displays the three-dimensional biosorption isotherm surfaces of the Ni^{2+}-Zn^{2+} bimetal system.

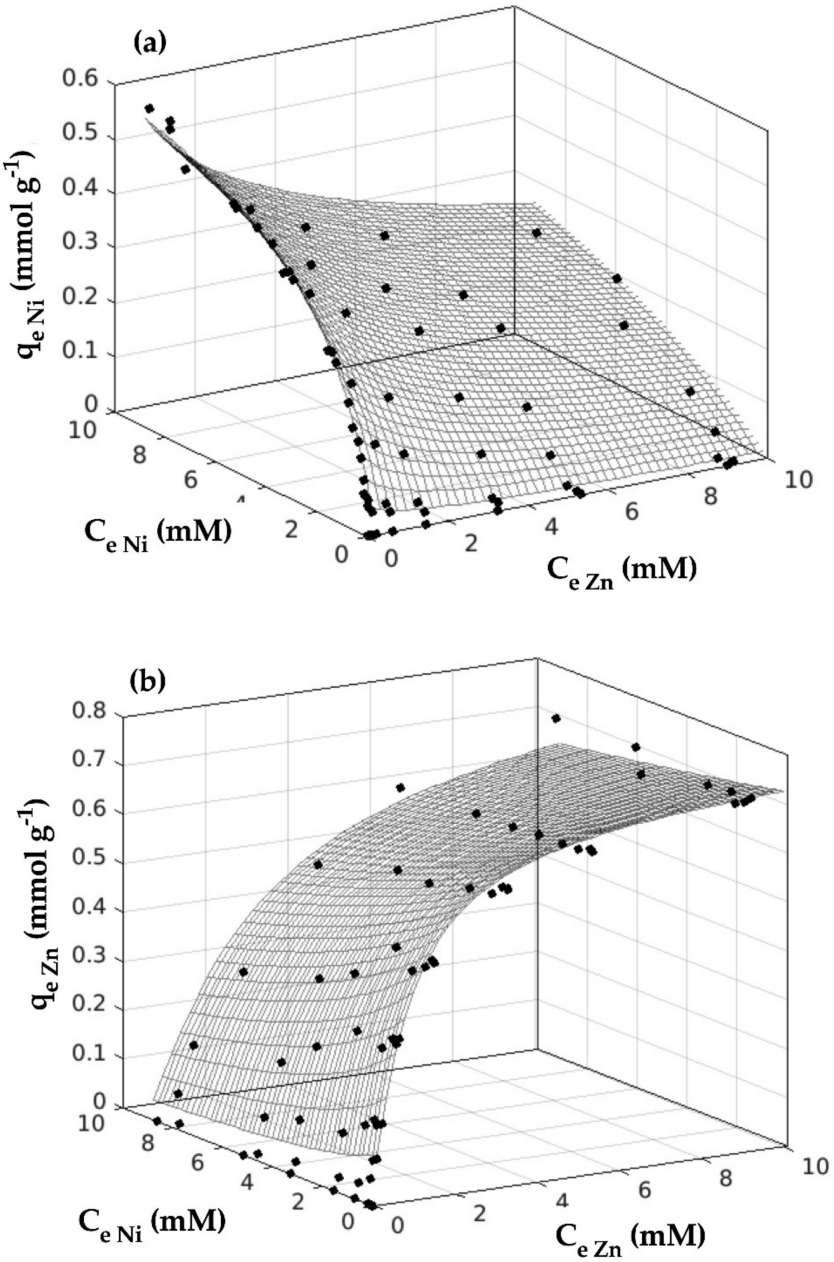

Figure 5. Isotherms of Ni^{2+} (**a**) and Zn^{2+} (**b**) biosorption on *Lemna gibba* in binary metal systems (• experimental data; — (mesh surface), modified Sips model prediction).

3D plots confirmed that biosorption of Ni^{2+} ions was negatively influenced to a great extent by Zn^{2+} ions present in aqueous solution (Figure 5a), whereas the presence of Ni^{2+} in the liquid phase had a less pronounced influence on Zn^{2+} biosorption (Figure 5b). This difference can be attributed to the competition between Ni^{2+} and Zn^{2+} ions for the same active biosorption sites on the *L. gibba* biomass

surface and to the higher affinity of *L. gibba* for Zn^{2+} than for Ni^{2+}. Moreover, these results clearly show that an antagonistic competitive effect occurs in the biosorption of each single heavy metal ion (Figure 5a,b), particularly at the high concentration range.

Table 6 reports the calculated parameter values of the different multicomponent isotherm models assayed in this work for the binary biosorption of Ni^{2+} and Zn^{2+} ions onto *L. gibba*, together with the corresponding error functions (i.e., R^2, *Sy.x*, *RMSE*, and *SSE* values).

Table 6. Isotherm model parameters for Ni^{2+} and Zn^{2+} biosorption in binary metal systems.

	Ni^{2+}	Zn^{2+}
Non-modified competitive Langmuir		
q_{max}Ni	0.982 ± 0.074	
q_{max}Zn		0.852 ± 0.022
B_{L}Ni	0.231 ± 0.053	0.231 ± 0.053
B_{L}Zn	0.875 ± 0.112	0.875 ± 0.112
R^2	0.935	0.985
SSE	0.122	0.067
Sy.x	0.045	0.033
RMSE	0.044	0.032
Modified Langmuir with interaction factor η		
q_{max}Ni	0.982 ± 0.074	
q_{max}Zn		0.852 ± 0.022
B_{L}Ni	0.231 ± 0.053	0.231 ± 0.053
B_{L}Zn	0.875 ± 0.112	0.875 ± 0.112
η_{Ni}	1.076 ± 0.049	1.237 ± 0.161
η_{Zn}	1.809 ± 0.206	1.041 ± 0.046
R^2	0.960	0.986
SSE	0.075	0.063
Sy.x	0.035	0.032
RMSE	0.034	0.031
Modified competitive Langmuir		
$q_{max\,Ni}'$	0.675 ± 0.02	
$q_{max\,Zn}'$		0.832 ± 0.015
B_{Ni}'	0.523 ± 0.045	0.194 ± 0.026
B_{Zn}'	0.74 ± 0.066	0.908 ± 0.063
R^2	0.985	0.986
SSE	0.028	0.061
Sy.x	0.021	0.032
RMSE	0.021	0.031
Extended Freundlich		
$K_{F\,Ni}$	0.253 ± 0.007	
$n_{F\,Ni}$	2.587 ± 0.069	
$K_{F\,Zn}$		0.382 ± 0.028
$n_{F\,Zn}$		3.705 ± 0.388
x_{Ni}	0.687 ± 0.067	
y_{Ni}	0.759 ± 0.075	
z_{Ni}	0.823 ± 0.055	
x_{Zn}		2.142 ± 0.285
y_{Zn}		0.074 ± 0.027
z_{Zn}		1.249 ± 0.211
R^2	0.980	0.978
SSE	0.037	0.095
Sy.x	0.025	0.040
RMSE	0.024	0.039

	Ni^{2+}	Zn^{2+}
Modified Sips		
$q_{max\,Ni}$	0.750 ± 0.048	
$B_{S\,Ni}$	0.488 ± 0.063	0.306 ± 0.115
$n_{S\,Ni}$	0.903 ± 0.048	0.970 ± 0.165
$q_{max\,Zn}$		0.764 ± 0.018
$B_{S\,Zn}$	0.941 ± 0.151	1.202 ± 0.123
$n_{S\,Zn}$	0.785 ± 0.050	1.195 ± 0.059
R^2	0.988	0.989
SSE	0.022	0.050
Sy.x	0.019	0.029
RMSE	0.018	0.028
Non-modified competitive Redlich-Peterson		
$K_{RP\,Ni}$	1.886 ± 0.523	
$A_{RP\,Ni}$	6.456 ± 2.038	6.456 ± 2.038
$b_{RP\,Ni}$	0.655 ± 0.012	0.655 ± 0.012
$K_{RP\,Zn}$		1.234 ± 0.098
$A_{RP\,Zn}$	2.028 ± 0.222	2.028 ± 0.222
$b_{RP\,Zn}$	0.885 ± 0.011	0.885 ± 0.011
R^2	0.903	0.440
SSE	0.182	2.526
Sy.x	0.055	0.207
RMSE	0.054	0.200
Modified Redlich–Peterson with interaction factor η		
$K_{RP\,Ni}$	1.886 ± 0.523	
$A_{RP\,Ni}$	6.456 ± 2.038	6.456 ± 2.038
$b_{RP\,Ni}$	0.655 ± 0.012	0.655 ± 0.012
$K_{RP\,Zn}$		1.234 ± 0.098
$A_{RP\,Zn}$	2.028 ± 0.222	2.028 ± 0.222
$b_{RP\,Zn}$	0.885 ± 0.011	0.885 ± 0.011
η_{Ni}	1.019 ± 0.04	28.292 ± 6.56
η_{Zn}	0.382 ± 0.036	0.868 ± 0.054
R^2	0.984	0.983
SSE	0.031	0.077
Sy.x	0.022	0.035
RMSE	0.022	0.034

The comparative analysis of the error function values indicates that several of the applied models can be used for the estimation of the biosorption behavior of Ni^{2+}-Zn^{2+} binary mixtures on *L. gibba*. However, the modified Sips model gives the best fitting for this binary metal system. The agreement between experimental results and those calculated by the modified Sips model is shown in Figure 5 (points and mesh surfaces, respectively). The modified Sips model predicted maximum capacities for Ni^{2+} and Zn^{2+} biosorption of 0.75 and 0.764 mmol g^{-1}, respectively, for the binary metal system.

3.5. FTIR Analysis

FTIR spectroscopy analyses were performed on raw (i.e., not loaded with Ni^{2+} or Zn^{2+} ions), Ni^{2+}-loaded, Zn^{2+}-loaded, and (Ni^{2+} + Zn^{2+})-loaded *L. gibba* samples to determine the chemical functional groups present on the *L. gibba* surface that might play a key role in the biosorptive removal of Ni^{2+} and Zn^{2+} ions from the liquid phases. To achieve this purpose, the FTIR spectrum of raw biosorbent was compared with that of Ni^{2+}-loaded, Zn^{2+}-loaded, and (Ni^{2+} + Zn^{2+})-loaded *L. gibba* (Figure 6).

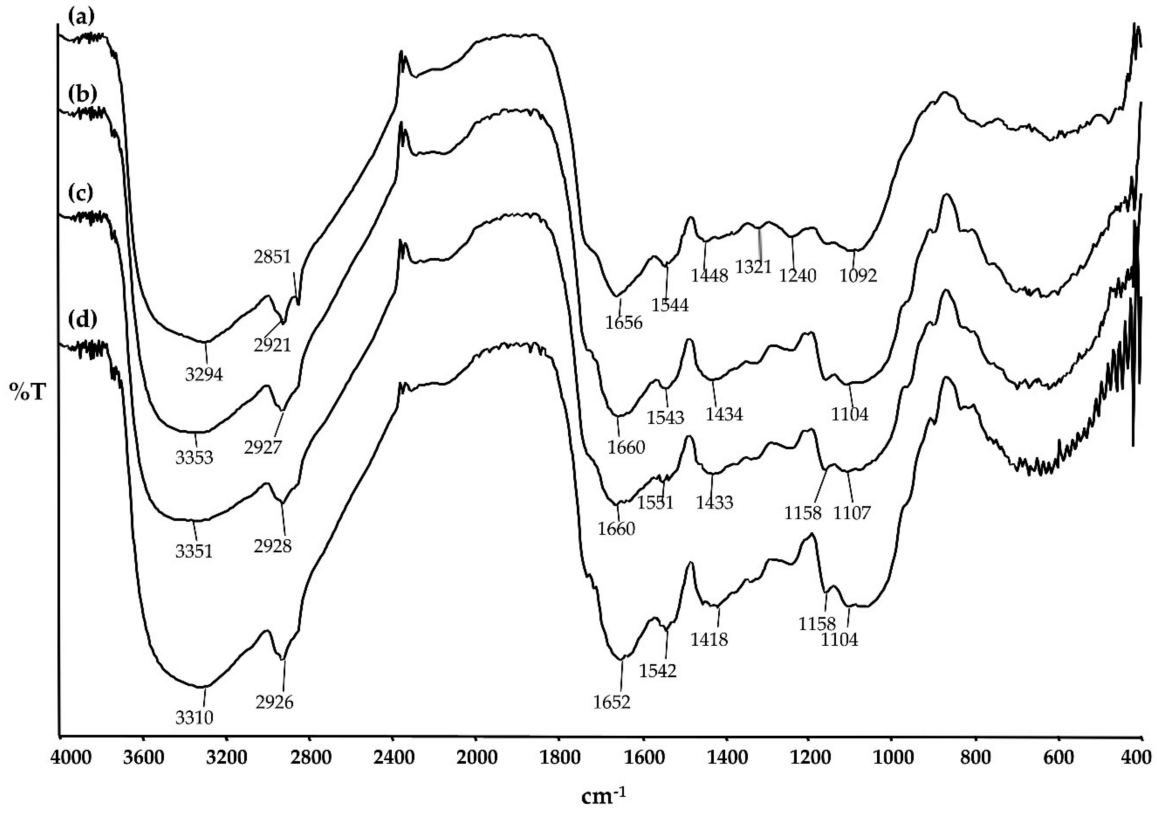

Figure 6. FTIR spectra of raw (**a**), Ni^{2+}-loaded (**b**), Zn^{2+}-loaded (**c**), and (Ni^{2+} + Zn^{2+})-loaded (**d**) *Lemna gibba*.

The abundant infrared absorption bands within the range of 4000–400 cm^{-1} in the FTIR spectrum of raw *L. gibba* is indicative of the complex chemical composition of its surface. The broad FTIR band at 3800–2800 cm^{-1}, with a minimum at 3294 cm^{-1}, corresponds to the stretching vibration of hydrogen-bonded –OH and –NH functional groups. This infrared absorption band is associated with the vibrations of the linked -OH groups in lignin, cellulose, and hemicellulose, which are present in Lemnaceae, and water adsorbed on the surface of lignocellulosic biomass [35,46]. Likewise, the -NH stretching vibration band in the FTIR spectrum of raw *L. gibba* indicated the presence of amino acids in the duckweed biomass, which are the building blocks of proteins. These polymeric compounds constitute approximately 29.26% of the dry biomass of *L. gibba*.

At approximately 2921 cm^{-1}, the absorption band is attributed to the stretching vibration of CH_2 and C-H functional groups found in lignin [35]. The absorption bands at approximately 1656 cm^{-1} and 1544 cm^{-1} are indicative of C=O stretching and N-H bending of amide I and amide II functional groups, respectively [35]. The C-O stretching of cellulose, hemicellulose, and proteins, and the -SO_3 stretching vibration of hemicelluloses, were detected at 1448 and 1240 cm^{-1}, respectively [35]. The absorption band of C-H vibration of cellulose and hemicellulose at approximately 1321 cm^{-1} [35,47] was also found in the FTIR spectrum of raw *L. gibba*. In addition, the FTIR band at 1092 cm^{-1} was assigned to the vibrations of O-H and C-O-C groups of polysaccharides [41].

After loading Ni^{2+}, Zn^{2+}, or (Ni^{2+} + Zn^{2+}) ions onto the raw *L. gibba* biosorbent, the FTIR spectra displayed several changes related to the polysaccharides present in the biosorbent. Among these changes was the shifting of the absorption band from 1448 to 1434, 1433, and 1418 cm^{-1} in the FTIR spectra of Ni^{2+}-loaded, Zn^{2+}-loaded, and (Ni^{2+} + Zn^{2+})-loaded *L. gibba*, respectively. Furthermore, the FTIR band at 1092 cm^{-1} shifted to 1104, 1107, and 1104 cm^{-1} in the FTIR spectra of Ni^{2+}-loaded, Zn^{2+}-loaded, and (Ni^{2+} + Zn^{2+})-loaded biosorbent, respectively. Likewise, the absorption band at 3294 cm^{-1} shifted to 3353, 3351, and 3310 cm^{-1} in the FTIR spectra of Ni^{2+}-loaded, Zn^{2+}-loaded, and (Ni^{2+} + Zn^{2+})-loaded *L. gibba*, respectively. It is well known that shifts in FTIR bands after metal biosorption are suggestive of interactions between the biosorbent's functional groups and metal ions [35]. Furthermore, another important change was the disappearance of the absorption band at 1321 cm^{-1} in the absorption spectra of Ni^{2+}-loaded, Zn^{2+}-loaded, and (Ni^{2+} + Zn^{2+})-loaded *L. gibba*. Considering the aforementioned assignments, these changes clearly denote the involvement of hemicellulose and cellulose of *L. gibba* in the biosorption of Ni^{2+} and Zn^{2+} ions.

3.6. SEM-EDX Analysis

SEM was employed to examine the physical morphology of the *L. gibba* surface before and after metal biosorption. SEM micrographs (Figure 7) displayed differences in surface morphology between the raw (Figure 7a) and the heavy metal-loaded *L. gibba* (Figure 7b–d).

The raw biosorbent showed a relatively regular surface morphology. Contrastingly, the morphology of the biosorbent surface changed after metal biosorption, becoming heterogeneous and smooth. These results are in agreement with other studies that have also found differences between the surface morphology of metal-unloaded and metal-loaded biosorbents [48,49].

Results of EDX analysis showed the presence of carbon, oxygen, nitrogen, sodium, magnesium, silicon, sulfur, chlorine, and potassium, and the absence of nickel and/or zinc on the *L. gibba* surface before interacting with heavy metals (Figure 7a). However, new Ni (Figure 7b), Zn (Figure 7c), and (Ni + Zn) (Figure 7d) peaks were observed on the biosorbent surface after interacting with Ni^{2+}, Zn^{2+}, and (Ni^{2+} + Zn^{2+}) ions.

Furthermore, SEM and elemental mappings of Ni^{2+} and Zn^{2+} on a particular surface spot after heavy metal biosorption are provided in Figure 8.

Bright spots denote the presence of nickel (Figure 8a,c) or zinc (Figure 8b,d) on the *L. gibba* surface. It is apparent that the biosorbed Ni and Zn ions were not distributed uniformly on the *L. gibba* surface, indicating that only some chemical functional groups present on the *L. gibba* surface were capable of biosorbing the divalent metal ions from the aqueous solutions. Therefore, SEM-EDX analysis confirmed the biosorption of Ni^{2+} and Zn^{2+} ions onto *L. gibba*.

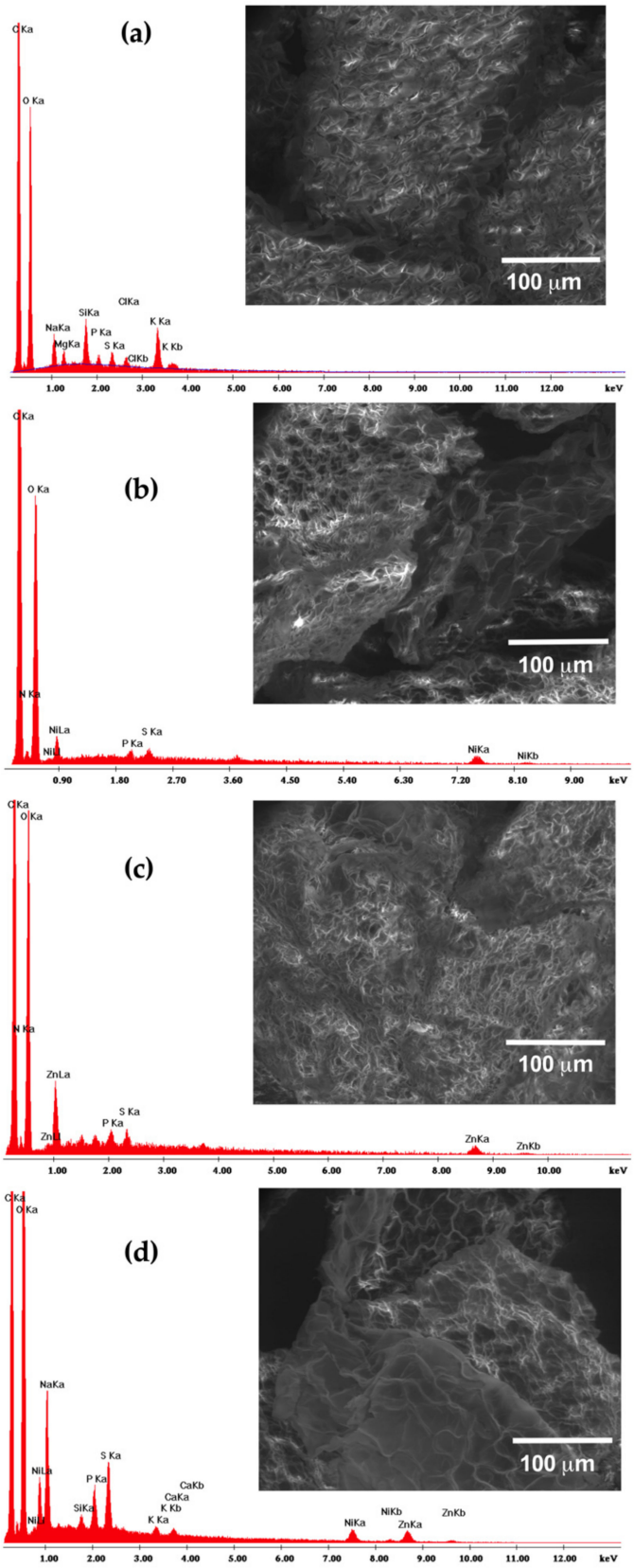

Figure 7. SEM-EDX micrographs of raw (**a**), Ni^{2+}-loaded (**b**), Zn^{2+}-loaded (**c**), and (Ni^{2+} + Zn^{2+})-loaded (**d**) *Lemna gibba*.

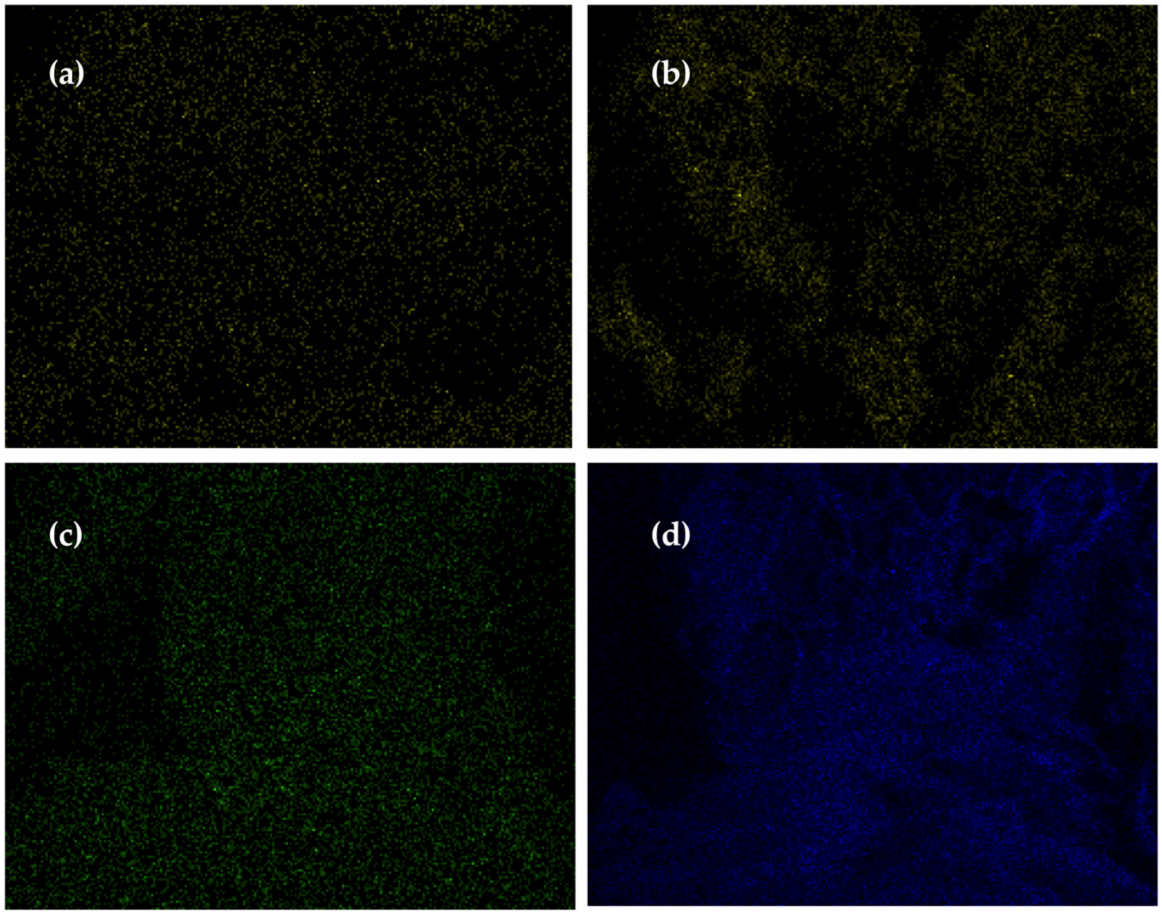

Figure 8. SEM/X-ray mapping of *Lemna gibba* loaded with Ni^{2+} (**a**) and Zn^{2+} (**b**) in single metal systems, and with Ni^{2+} (**c**) and Zn^{2+} (**d**) in binary metal systems.

4. Conclusions

This study demonstrates that *L. gibba* is an effective and promising biosorbent for the simultaneous removal of Ni^{2+} and Zn^{2+} ions from liquid solutions. Solution pH value has a significant influence on Ni^{2+} and Zn^{2+} biosorption by *L. gibba*, both in the single and in binary metal systems. The maximum levels of divalent heavy metal biosorption occurred at pH 6.0. In both the single and binary metal biosorption systems, the affinity of *L. gibba* for Zn^{2+} ions was greater than for Ni^{2+} ions. In the binary metal biosorption systems, it was observed that Zn^{2+} ions exhibited a strong antagonistic effect on Ni^{2+} biosorption. Contrastingly, the interference of Ni^{2+} ions on Zn^{2+} biosorption was less significant. Redlich–Peterson and Freundlich models were found to better fit Ni^{2+} equilibrium data, whereas Redlich–Peterson and Langmuir models provided the best fit of the Zn^{2+} equilibrium data in single metal biosorption systems. The simultaneous biosorption of Ni^{2+} and Zn^{2+} ions onto the *L. gibba* was adequately and satisfactorily described by the modified competitive Sips model. FTIR results suggest that Ni^{2+} and Zn^{2+} ions bind to *L. gibba*'s polysaccharides, and SEM-EDX analysis validated the presence of the heavy metals on the surface of duckweed. Both Ni^{2+} and Zn^{2+} ions could be desorbed easily from heavy metal-loaded *L. gibba* using acid solutions, and facilitate heavy metal recovery and biosorbent regeneration.

Author Contributions: Conceptualization, E.C.-U.; methodology, L.M.-B., C.M.F.-O. and E.C.-U.; software, L.M.-B.; validation, L.M.-B.; formal analysis, L.M.-B., C.M.F.-O. and E.C.-U.; investigation, L.M.-B.; resources, E.C.-U.; writing—original draft preparation, L.M.-B. and E.C.-U.; writing—review and editing, L.M.-B., C.M.F.-O. and E.C.-U.; visualization, L.M.-B.; supervision, E.C.-U.; project administration, E.C.-U.; funding acquisition, E.C.-U. All authors have read and agreed to the published version of the manuscript.

Funding: This research was funded by the Instituto Politécnico Nacional, Secretaría de Investigación y Posgrado, project number: SIP20201439.

Acknowledgments: The authors acknowledge the technical support provided by the Centro de Nanociencias y Micro y Nanotecnologías, IPN. L.M.-B. and E.C.-U. hold grants from EDI-IPN, COFAA-IPN, and SNI-CONACYT.

Conflicts of Interest: The authors declare no conflict of interest.

References

1. Nys, C.; Asselman, J.; Hochmuth, J.D.; Janssen, C.R.; Blust, R.; Smolders, E.; De Schamphelaere, K.A. Mixture toxicity of nickel and zinc to Daphnia magna is noninteractive at low effect sizes but becomes synergistic at high effect sizes. *Environ. Toxicol. Chem.* **2015**, *34*, 1091–1102. [CrossRef] [PubMed]
2. Meng, L.; Lin, D.; Wang, J.; Zeng, Y.; Liu, Y.; Lu, X. Electrochemically Activated Nickel–Carbon Composite as Ultrastable Cathodes for Rechargeable Nickel–Zinc Batteries. *ACS Appl. Mater. Interfaces* **2019**, *11*, 14854–14861. [CrossRef]
3. Yang, S.; Bo, M.; Peng, C.; Li, Y.; Li, Y. Three-electrode flexible zinc-nickel battery with black phosphorus modified polymer electrolyte. *Mater. Lett.* **2018**, *233*, 118–121. [CrossRef]
4. Malamis, S.; Katsou, E. A review on zinc and nickel adsorption on natural and modified zeolite, bentonite and vermiculite: Examination of process parameters, kinetics and isotherms. *J. Hazard. Mater.* **2013**, *252*, 428–461. [CrossRef] [PubMed]
5. Bashmakova, E.B.; Pashkovskiy, P.P.; Radyukina, N.L.; Kuznetsov, V.V. Possible mechanism of iron deficit development in Mimulus guttatus plants exposed to joint action of nickel and zinc salts. *Russ. J. Plant Physiol.* **2015**, *62*, 761–771. [CrossRef]
6. Brocato, J.; Costa, M. 10th NTES Conference: Nickel and arsenic compounds alter the epigenome of peripheral blood mononuclear cells. *J. Trace Elements Med. Biol.* **2015**, *31*, 209–213. [CrossRef]
7. Maroney, M.J.; Ciurli, S. Nonredox Nickel Enzymes. *Chem. Rev.* **2013**, *114*, 4206–4228. [CrossRef]
8. Nriagu, J. Zinc Toxicity in Humans. In *Encyclopedia of Environmental Health*; Elsevier BV: Amsterdam, The Netherlands, 2011; Volume 5, pp. 801–807.
9. Martinez, R.S.; Sáenz, M.E.; Alberdi, J.L.; Di Marzio, W.D. Comparative ecotoxicity of single and binary mixtures exposures of nickel and zinc on growth and biomarkers of Lemna gibba. *Ecotoxicology* **2019**, *28*, 686–697. [CrossRef]
10. De Figuerêdo, L.P.; Nilin, J.; Da Silva, A.Q.; Damasceno, É.P.; Loureiro, S.; Costa-Lotufo, L.V. Zinc and nickel binary mixtures act additively on the tropical mysid Mysidopsis juniae. *Mar. Freshw. Res.* **2016**, *67*, 301–308. [CrossRef]
11. Aranda-García, E.; Cristiani-Urbina, E. Kinetic, Equilibrium, and Thermodynamic Analyses of Ni(II) Biosorption from Aqueous Solution by Acorn Shell of Quercus crassipes. *Water Air Soil Pollut.* **2018**, *229*, 119. [CrossRef]
12. Aranda-García, E.; Cristiani-Urbina, E. Effect of pH on hexavalent and total chromium removal from aqueous solutions by avocado shell using batch and continuous systems. *Environ. Sci. Pollut. Res.* **2019**, *26*, 3157–3173. [CrossRef] [PubMed]
13. Arim, A.L.; Guzzo, G.; Quina, M.J.; Ferreira, L.M.G. Single and binary sorption of Cr(III) and Ni(II) onto modified pine bark. *Environ. Sci. Pollut. Res.* **2018**, *25*, 28039–28049. [CrossRef] [PubMed]
14. Thangaraj, V.; Aravamudan, K.; Lingam, R.; Subramanian, S. Individual and simultaneous adsorption of Ni (II), Cd (II), and Zn (II) ions over polyamide resin: Equilibrium, kinetic and thermodynamic studies. *Environ. Prog. Sustain. Energy* **2019**, *38*, S340–S351. [CrossRef]
15. León, M.D.C.C.-D.; Flores-Alamo, N.; Solache-Ríos, M.J.; De La Rosa-Gómez, I.; Díaz-Campos, G. Lead and Copper Adsorption Behaviour by Lemna gibba: Kinetic and Equilibrium Studies. *CLEAN—Soil Air Water* **2017**, *45*, 1600357. [CrossRef]
16. Babativa, D.F.R.; Ramírez, A.J.E. Comparación de las características poblacionales de Lemna minuta (ARACEAE: LEMNOIDEAE) en tres medios de cultivo. *Rev. Colomb. Biotecnol.* **2018**, *20*, 84–96. [CrossRef]
17. Topal, M.; Obek, E.; Şenel, G.U.; Topal, E.I.A. Removal of tetracycline antibiotic by Lemna gibba L. from aqueous solutions. *Water Environ. J.* **2020**, *34*, 37–44. [CrossRef]
18. Mkandawire, M.; Dudel, E.G. Are Lemna spp. effective phytoremediation agents? *Bioremediat. Biodivers. Bioavail.* **2007**, *1*, 56–71.

19. Azer, S. Taxonomic revision of genus Lemna L. (Lemnaceae Gray) in Egypt. *Ann. Agric. Sci.* **2013**, *58*, 257–263. [CrossRef]
20. Tang, Y.; Chen, L.; Wei, X.; Yao, Q.; Li, T. Removal of lead ions from aqueous solution by the dried aquatic plant, Lemna perpusilla Torr. *J. Hazard. Mater.* **2013**, *244*, 603–612. [CrossRef]
21. Reyes-Ledezma, J.L.; Uribe-Ramírez, D.; Cristiani-Urbina, E.; Morales-Barrera, L. Biosorptive removal of acid orange 74 dye by HCl-pretreated Lemna sp. *PLoS ONE* **2020**, *15*, e0228595. [CrossRef] [PubMed]
22. Horwitz, W.; Latimer, G.W., Jr. *Official Methods of Analysis of AOAC International*, 18th ed.; AOAC International: Gaithersburg, MD, USA, 2005.
23. Filipović-Kovačević, Ž.; Sipos, L.; Briški, F. Biosorption of chromium, copper, nickel and zinc ions onto fungal pellets of Aspergillus niger 405 from aqueous solutions. *Food Technol. Biotechnol.* **2000**, *38*, 211–216.
24. Gupta, V.K.; Suhas; Nayak, A.; Agarwal, S.; Chaudhary, M.; Tyagi, I. Removal of Ni (II) ions from water using scrap tire. *J. Mol. Liq.* **2014**, *190*, 215–222. [CrossRef]
25. Netzahuatl-Muñoz, A.R.; Cristiani-Urbina, M.D.C.; Cristiani-Urbina, E. Chromium Biosorption from Cr(VI) Aqueous Solutions by Cupressus lusitanica Bark: Kinetics, Equilibrium and Thermodynamic Studies. *PLoS ONE* **2015**, *10*, e0137086. [CrossRef]
26. Oliveira, E.; Montanher, S.; Andrade, A.; Nóbrega, J.D.A.; Rollemberg, M. Equilibrium studies for the sorption of chromium and nickel from aqueous solutions using raw rice bran. *Process. Biochem.* **2005**, *40*, 3485–3490. [CrossRef]
27. Febrianto, J.; Kosasih, A.N.; Sunarso, J.; Ju, Y.-H.; Indraswati, N.; Ismadji, S. Equilibrium and kinetic studies in adsorption of heavy metals using biosorbent: A summary of recent studies. *J. Hazard. Mater.* **2009**, *162*, 616–645. [CrossRef]
28. Vijayaraghavan, K.; Padmesh, T.; Palanivelu, K.; Manikam, V. Biosorption of nickel(II) ions onto Sargassum wightii: Application of two-parameter and three-parameter isotherm models. *J. Hazard. Mater.* **2006**, *133*, 304–308. [CrossRef] [PubMed]
29. Aksu, Z.; Açikel, Ü.; Kabasakal, E.; Tezer, S. Equilibrium modelling of individual and simultaneous biosorption of chromium(VI) and nickel(II) onto dried activated sludge. *Water Res.* **2002**, *36*, 3063–3073. [CrossRef]
30. Srivastava, V.C.; Mall, I.D.; Mishra, I.M. Equilibrium modelling of single and binary adsorption of cadmium and nickel onto bagasse fly ash. *Chem. Eng. J.* **2006**, *117*, 79–91. [CrossRef]
31. McKay, G.; Porter, J. A Comparison of Langmuir Based Models for Predicting Multicomponent Metal Ion Equilibrium Sorption Isotherms on Peat. *Process. Saf. Environ. Prot.* **1997**, *75*, 171–180. [CrossRef]
32. Luna, A.S.; Costa, A.L.H.; Da Costa, A.C.A.; Henriques, C.A. Competitive biosorption of cadmium(II) and zinc(II) ions from binary systems by Sargassum filipendula. *Bioresour. Technol.* **2010**, *101*, 5104–5111. [CrossRef]
33. Aksu, Z.; Akpinar, D. Competitive biosorption of phenol and chromium(VI) from binary mixtures onto dried anaerobic activated sludge. *Biochem. Eng. J.* **2001**, *7*, 183–193. [CrossRef]
34. Muhammad; Chuah, T.; Robiah, Y.; Suraya, A.; Choong, T. Single and binary adsorptions isotherms of Cd(II) and Zn(II) on palm kernel shell based activated carbon. *Desalin. Water Treat.* **2011**, *29*, 140–148. [CrossRef]
35. Guerrero-Coronilla, I.; Aranda-Garcia, E.; Cristiani-Urbina, E. Biosorption of Metanil Yellow Dye from Aqueous Solutions by the Entire Water Hyacinth Plant (Eichhornia crassipes) and Its Vegetative Organs. *Environ. Eng. Manag. J.* **2019**, *18*, 1671–1682. [CrossRef]
36. Hach Company. *Hach Water Analysis Handbook*; Hach Company: Hach, Loveland, 2008.
37. Schmid, R.; Landolt, E. Biosystematic Investigations in the Family of Duckweeds (Lemnaceae). *TAXON* **1987**, *36*, 781. [CrossRef]
38. Landesman, L. Effects of herbivory and competition of growth of Lemnaceae in systems for wastewater treatment and livestock feed production. Ph.D. Thesis, University of Louisiana, Lafayette, LA, USA, 2000; p. 150.
39. Salam, O.E.A.; Reiad, N.A.; Elshafei, M.M. A study of the removal characteristics of heavy metals from wastewater by low-cost adsorbents. *J. Adv. Res.* **2011**, *2*, 297–303. [CrossRef]
40. Liu, Y.; Fan, T.; Zeng, G.-M.; Li, X.; Tong, Q.; Ye, F.; Zhou, M.; Xu, W.-H.; Huang, Y.-E. Removal of cadmium and zinc ions from aqueous solution by living Aspergillus niger. *Trans. Nonferrous Met. Soc. China* **2006**, *16*, 681–686. [CrossRef]

41. Saygideger, S.; Gülnaz, O.; Istifli, E.S.; Yucel, N. Adsorption of Cd(II), Cu(II) and Ni(II) ions by Lemna minor L.: Effect of physicochemical environment. *J. Hazard. Mater.* **2005**, *126*, 96–104. [CrossRef]
42. Quintelas, C.; Rocha, Z.; Silva, B.; Fonseca, B.; Figueiredo, H.; Tavares, M. Removal of Cd(II), Cr(VI), Fe(III) and Ni(II) from aqueous solutions by an E. coli biofilm supported on kaolin. *Chem. Eng. J.* **2009**, *149*, 319–324. [CrossRef]
43. Şengil, I.A.; Ozacar, M. Competitive biosorption of Pb^{2+}, Cu^{2+} and Zn^{2+} ions from aqueous solutions onto valonia tannin resin. *J. Hazard. Mater.* **2009**, *166*, 1488–1494. [CrossRef]
44. Sağ, Y.; Akçael, B.; Kutsal, T. Evaluation, interpretation, and representation of three-metal biosorption equilibria using a fungal biosorbent. *Process. Biochem.* **2001**, *37*, 35–50. [CrossRef]
45. Sedlakova-Kadukova, J.; Horváthová, H. Biosorption of Copper, Zinc and Nickel From Multi-Ion Solutions. *Nova Biotechnol. Chim.* **2012**, *11*, 125–132. [CrossRef]
46. Li, C.; Li, D.; Feng, J.; Fan, X.; Chen, S.; Zhang, D.; He, R. Duckweed (Lemna minor) is a novel natural inducer of cellulase production in Trichoderma reesei. *J. Biosci. Bioeng.* **2019**, *127*, 486–491. [CrossRef] [PubMed]
47. Zhang, S.; Chen, T.; Li, W.; Dong, Q.; Xiong, Y. Physicochemical properties and combustion behavior of duckweed during wet torrefaction. *Bioresour. Technol.* **2016**, *218*, 1157–1162. [CrossRef] [PubMed]
48. Blanes, P.S.; Bordoni, M.E.; Gonzalez, J.C.; García, S.I.; Atria, A.M.; Sala, L.F.; Bellú, S.E. Application of soy hull biomass in removal of Cr(VI) from contaminated waters. Kinetic, thermodynamic and continuous sorption studies. *J. Environ. Chem. Eng.* **2016**, *4*, 516–526. [CrossRef]
49. Kuppusamy, S.; Thavamani, P.; Megharaj, M.; Venkateswarlu, K.; Lee, Y.B.; Naidu, R. Oak (Quercus robur) Acorn Peel as a Low-Cost Adsorbent for Hexavalent Chromium Removal from Aquatic Ecosystems and Industrial Effluents. *Water Air Soil Pollut.* **2016**, *227*, 62. [CrossRef]